UCRL-16253

University of California

Ernest O. Lawrence Radiation Laboratory

TWO-WEEK LOAN COPY

This is a Library Circulating Copy which may be borrowed for two weeks. For a personal retention copy, call Tech. Info. Division, Ext. 5545

TIME REVERSAL, THE FORM FACTOR RATIO, AND THE BRANCHING RATIO IN $K^+_{\mu 3}$ DECAY

Berkeley, California

DISCLAIMER

This document was prepared as an account of work sponsored by the United States Government. While this document is believed to contain correct information, neither the United States Government nor any agency thereof, nor the Regents of the University of California, nor any of their employees, makes any warranty, express or implied, or assumes any legal responsibility for the accuracy, completeness, or usefulness of any information, apparatus, product, or process disclosed, or represents that its use would not infringe privately owned rights. Reference herein to any specific commercial product, process, or service by its trade name, trademark, manufacturer, or otherwise, does not necessarily constitute or imply its endorsement, recommendation, or favoring by the United States Government or any agency thereof, or the Regents of the University of California. The views and opinions of authors expressed herein do not necessarily state or reflect those of the United States Government or any agency thereof or the Regents of the University of California.

Special thesis

UCRL-16253

UNIVERSITY OF CALIFORNIA

Lawrence Radiation Laboratory
Berkeley, California

AEC Contract No. W-7405-eng-48

TIME REVERSAL, THE FORM FACTOR RATIO, AND THE BRANCHING RATIO IN $K^+_{\mu 3}$ DECAY

Carl L. Sandler

(Ph. D. Thesis)

June 1965

TIME REVERSAL, THE FORM FACTOR RATIO, AND THE BRANCHING RATIO IN $K^+_{\mu 3}$ DECAY

Table of Contents

Abstract v

I. Introduction 1

II. Theory and Its Application in Analysis 6

III. Experimental Procedure 11

A. Exposure 11

B. Beam 12

C. Range-Energy Relations 13

D. Scanning 13

E. Measuring and Data Processing 18

IV. Analysis 20

A. General Discussion 20

B. Background Corrections 29

C. Geometrical Corrections 35

D. Analysis Functions 37

V. Results 45

VI. Conclusion 48

Acknowledgments 50

References 52

Appendices 59

A. Some Algebraic Expressions 59

B. Range-Momentum Tables for C_3F_8 60

C. List of Tables and Figure Captions 64

TIME REVERSAL, THE FORM FACTOR RATIO, AND THE BRANCHING RATIO IN $K^+_{\mu 3}$ DECAY

Carl L. Sandler

Lawrence Radiation Laboratory
University of California
Berkeley, California

June 1965

ABSTRACT

The muon kinetic energy spectrum and the branching ratio have been measured in the $K^+_{\mu 3}$ decay, $K^+ \rightarrow \pi^0 + \mu^+ + \nu$. Pictures of K^+ mesons stopping in the Berkeley 30-inch heavy-liquid bubble chamber filled with C_3F_8 yielded 914 observed events with muon kinetic energy $41 \leq T_\mu \leq 94$ MeV. Assuming time reversal invariance, we fitted the data with a one parameter (V - A) theory to determine from the spectral shape the parameter ξ, the ratio of the form factors, and to determine from the area under the normalized, best-fitting spectral curve, the $K^+_{\mu 3}$ branching ratio, $BR_{K_{\mu 3}}$. In the analysis we used the χ^2 test of hypothesis to determine that the best solution for the purely real or purely imaginary parameter ξ occurred when $\xi = 0^{+2.0}_{-1.4}$, at the point where χ^2 was a minimum. The total area under the theoretical spectral curve, parameterized by the above value of ξ and normalized over the region measured to the number of experimental $K^+_{\mu 3}$ events, gave the total number of $K^+_{\mu 3}$ events in the experiment. We obtained the $K^+_{\mu 3}$ branching ratio, $BR_{K_{\mu 3}} = (2.93 \pm 0.23)\%$, from the ratio of the total number of $K^+_{\mu 3}$ events to the total number of K^+ mesons, determined from counting K^+_τ decays. These values of ξ and $BR_{K_{\mu 3}}$ represent the best statistical estimates in this experiment of the true values of these parameters. A determination of the values of ξ compatible with

the data showed that at the 95% confidence level, all values of ξ from -4.0 to +10.0 (the highest value tested) were possible. The $K^+_{\mu 3}$ branching ratio is rather insensitive to variations in ξ and over the range $-4.0 \leq \xi \leq +10.0$, assumes the values $2.88 \leq BR_{K_{\mu 3}} \leq 3.09\%$. If μe-universality is assumed, along with the published experimental average of the K_{e3} branching ratio, $BR_{K_{e3}} = (4.8 \pm 0.32)\%$, an equation relating $BR_{K_{\mu 3}}$ to ξ can be established. The intersection of this equation with the curve determined by the experimentally obtained dependence of $BR_{K_{\mu 3}}$ on ξ enables one to simultaneously determine rather restricted values for ξ and the $K^+_{\mu 3}$ branching ratio. These are $\xi = -0.4 \pm 0.9$ and $BR_{K_{\mu 3}} = (2.9 \pm 0.3)\%$. On the basis of this solution, theories of the $K^+_{\mu 3}$ decay mechanism which predict that the absolute value of ξ is large can be rejected, but no discrimination can be made among those theories that predict ξ near zero.

With ξ assumed complex, the same data has been analyzed with a two parameter maximum likelihood function to determine ξ_{RE} and ξ_{IM}. The likelihood function is non-Gaussian, but its sensitivity can be indicated by quoting the customary $e^{-0.5}$ and $e^{-2.0}$ of the maximum value:

$$\text{For } L(\xi_{RE}, \xi_{IM}) = e^{-0.5} L_{MAX}, \ \xi_{RE} = 0^{+1.6}_{-1.2}, \text{ and } \xi_{IM} = 0 \pm 1.4;$$

$$L(\xi_{RE}, \xi_{IM}) = e^{-2.0} L_{MAX}, \ \xi_{RE} = 0^{+3.6}_{-2.1}, \text{ and } \xi_{IM} = 0 \pm 2.9.$$

The likelihood solutions are consistent with the time reversal invariance requirement that $\xi_{IM} = 0$.

I. INTRODUCTION

We have measured the muon kinetic energy spectrum and branching ratio in the strangeness-changing $K^+_{\mu 3}$ decay:

$$K^+ \rightarrow \pi^0 + \mu^+ + \nu.$$

The data was obtained from pictures taken of K^+ mesons stopping in the Berkeley 30-inch heavy-liquid bubble chamber filled with C_3F_8.

The purpose of this experiment was to determine:

(a) The mechanism of the $K^+_{\mu 3}$ decay.

(b) The $K^+_{\mu 3}$ branching ratio.

(c) Whether time reversal invariance holds in this strangeness-changing decay.

The spectra and the branching ratios of the three-body leptonic decay modes are important experimental checks on the present weak interaction theories[1,2]. Assuming time reversal invariance, we investigated the mechanism of the $K^+_{\mu 3}$ decay by fitting the shape of the muon decay spectrum by a single parameter $\xi \equiv f_-/f_+$, the ratio of the form factors. Theoretical calculations have been done which calculate the value of ξ assuming different models for the decay interaction. Most theoretical models[3-7] predict $-0.8 < \xi < +0.6$; an exception is the theory of Schwinger[8] which requires $\xi = -6.6$. In the summer of 1963, when this experiment was begun, there was disagreement in the experimental results for the measured value of ξ[9-11]. A paper by Zweig[12] attempted to reconcile these differences within a single theory. However, the results of our work[13,14] as well as recent measurements by other workers[15-20], indicate that the magnitude of ξ is small--near zero. (See Table I for a summary of experimental papers.)

We have determined the $K^+_{\mu 3}$ branching ratio by finding the total area

under the theoretical muon spectral curve which best fitted the data. The spectral curve was normalized to the data over the region measured and parameterized by that value of ξ which gave the best fit to the muon spectral shape. The total number of K^+ mesons present in the film scanned for $K^+_{\mu 3}$ events was determined by normalizing to K^+_τ decays. The value obtained for the branching ratio is consistent with recent measurements by the groups at Torino[17], Michigan[21] and Wisconsin[22]. A summary of the experimental measurements of the $K^+_{\mu 3}$ branching ratio is given in Reference 23.

It is important to test time reversal invariance in $K^+_{\mu 3}$ decay, especially because of a recent apparent violation of CP invariance in K^o_2 decay[24]. Most of the theoretical models[25-29] advanced to explain $K^o_2 \rightarrow \pi^+ + \pi^-$ decay, require that there be no violation of time reversal invariance in $K^+_{\mu 3}$ decay. Cabibbo's original proposal[30] on SU(3) restrictions for weak interactions required a violation of time reversal invariance in $K^+_{\mu 3}$ decay, but did not specify how large a violation. His more recent proposal[31] on C violations in strong and weak interactions requires no time reversal violation in $K^+_{\mu 3}$ decay larger than one to two percent in the limit of exact SU(3) symmetry. To test whether time reversal invariance holds in $K^+_{\mu 3}$ decay, we assumed that the form factor ratio ξ is complex, and then did a two parameter maximum likelihood analysis of the muon spectral data. Values were obtained for Re ξ and Im ξ. Time reversal invariance requires that Im $\xi = 0$, and the analysis results[32] were consistent with this criterion. Other work by our Berkeley group, in collaboration with Wisconsin and Bari, on the transverse polarization of the μ^+ in $K^+_{\mu 3}$ decay[33] and on the $K^+_{\mu 3}$ $\pi^o - \mu^+$ Dalitz plot analysis[22], corroborates the results for the complex value of ξ. The Torino group[34] has recently increased its statistics on the μ^+ spectrum and extended

its μ^+ spectral analysis to evaluate Im ξ. The group at Michigan[35] has also extended its μ^+ spectral analysis to evaluate Im ξ. Both groups obtain values compatible with those presented in this paper.

The following section describes the phenomenologically-based theory used in analysis. Subsequent sections describe the method of obtaining, processing, and analyzing the data, and then follow the results and conclusions.

TABLE I. Summary of Experimental Papers

Introduction

In the literature, the experiments done on $K^+_{\mu 3}$ decay, $K^+ \rightarrow \pi^o + \mu^+ + \nu$, have included measurements of:

(1) The μ^+ kinetic energy spectrum

(2) The μ^+ longitudinal, transverse, and total polarization

(3) The π^o and μ^+ spectra and angular correlations

(4) The $K^+_{\mu 3}$ branching ratio.

A consistent theory must show agreement among all these different types of experiments, for example, by predicting the same value of the decay parameter $\xi \equiv f_-/f_+$, the ratio of the form factors. In the table which follows, all experiments have used a pure vector coupling based on a one or two parameter (V - A) theory, depending on whether ξ is assumed real or complex. We summarize the measurements of ξ based on the assumption of constant form factors.

A knowledge of $R \equiv BR_{K_{\mu 3}}/BR_{K_{e3}}$ (the ratio of the $K^+_{\mu 3}$ to K^+_{e3} branching ratios) and assumption of μe-universality determine an equation for ξ which restricts the real value of ξ to near zero or to large negative numbers. Measurements of the μ^+ spectrum are capable of discriminating between these two solutions. Table I gives the values of both ξ and R for those experiments which use this approach.

Symbols

$P^{\parallel}_{\mu} = \mu^+$ longitudinal polarization ; $P^{\perp}_{\mu} = \mu^+$ transverse polarization

B.C. = Bubble Chamber ; T = Kinetic Energy

Reference and Technique	Method	T_μ (MeV) Low – High	Number of Events	ξ - Value
1. This experiment [32] (30 in. Berkeley B. C. Freon (C_3F_8))	μ^+ spectrum	(41 - 94)	914 observed (820 after corrections)	Assuming ξ real, $\xi = 0^{+2.0}_{-1.4}$, also find $BR_{K_{\mu 3}} = (2.93 \pm 0.23)\%$ Assuming ξ complex, $\xi_{RE} = 0^{+1.6}_{-1.2}$, $\xi_{IM} = 0 \pm 1.4$
	μ^+ spectrum & $BR_{K_{\mu 3}}$, with $BR_{K_{e3}} = (4.8 \pm 0.32)\%$			$\xi = -0.4 \pm 0.9$ $BR_{K_{\mu 3}} = (2.9 \pm 0.3)\%$
	μ^+ spectrum & $R = 0.60 \pm 0.07$			For $\xi_{IM} = 0$, $\xi_{RE} = -0.35^{+0.60}_{-0.76}$, (or $\xi = -6.21^{+0.60}_{-0.76}$)
2. U. Camerini et. al. [32] (30 in. Berkeley B. C. Freon (C_3F_8))	μ^+ spectrum	(42 - 94)	2654	Combined data, $\xi_{RE} = -0.30 \pm 0.65$, $\xi_{IM} = 0 \pm 0.85$
	$P_\mu^{\parallel}$ from ref. 19	(38 - 96)	2988	
	$\langle P_\mu^{\perp} \rangle = 0.04 \pm 0.35$	$T_\mu > 30$ $T_\pi < 110$	619	Assuming $\xi_{RE} = -0.30 \pm 0.65$, $\xi_{IM} = 0.2 \pm 1.8$
				The combined value of ξ_{IM}, $\xi_{IM} = 0.05 \pm 0.75$
3. V. Bisi et. al. [17] (81cm Saclay B. C. (H_2) 1m Ecole Polytechnique B. C. (Propane & Freon))	μ^+ spectrum	(5 - 35) (15-95) (105-134)	670 550 } 1220	Assuming ξ real, $\xi > -3$
	μ^+ spectrum & $BR_{K_{\mu 3}}$, with $BR_{K_{e3}} = (5.0 \pm 0.5)\%$			$\xi = 0 \pm 1$ $BR_{K_{\mu 3}} = (3.5 \pm 0.3)\%$
	μ^+ spectrum & $R = 0.74 \pm 0.08$			$\xi = 0.3 \pm 0.8$, (or $\xi = -7.1 \pm 0.8$)

TABLE I. Summary of Experimental Papers

Reference and Technique	Method	T_μ (MeV) Low	High	Number of Events	ξ - Value
3. (continued)					
1m Ecole Polytechnique B.C. (Propane & Freon)	μ^+ spectrum	(25 - 95)		714(includes some of the 550 above)	Assuming ξ real, $\xi > -3.3$ (χ^2 probability > 5%) also find $BR_{K_{\mu 3}} = (3.45 \pm 0.20)\%$
1m Ecole Polytechnique B.C. (Freon)				1357	Assuming ξ complex, $\xi_{RE} = -0.75 \pm 0.50$, $\xi_{IM} = 3.5 \pm 0.50$
	μ^+ spectrum & $R = 0.73 \pm 0.06$				$\xi = 0.6 \pm 0.5$, (or $\xi = -7.3 \pm 0.5$)
4. G. Jensen, et. al.[15,35] (12 in. Xe B.C.)	μ^+ & π^o spectra & angular correlations	(T_μ = (12-85) effectively) T_{π^o} = (0-115)		141	Assuming ξ complex, $0 \leq \lvert \xi_{IM} \rvert \leq 2.4$ at 90% confidence level $\xi_{RE} = -1.2 \pm 1.0$
5. G. Giacomelli, et. al.[16] (Nuclear Emulsion)	μ^+ spectrum & $R = 0.75 \pm 0.07$	(0 - 28)		87	$\xi = 0.7 \pm 0.5$, (or $\xi = -7.2 \pm 0.6$)
6. G. Gidal, et. al.[14] 30 in. Berkeley B.C. Freon (C_3F_8)	μ^+ & π^o spectra & angular correlations	T_μ = (15-85) T_{π^o} = (0-115)		138	$\xi = 1.3 \pm 0.9$ or $\xi = -5.2 \pm 0.7$ A weighted mean of this solution with the solution from ref. 19 gives: $\xi = 0.6 \pm 0.7$ or $\xi = -4.7 \pm 0.6$

-5-

7. A. Boyarksi, et. al.[10] (Scintillating Hodoscope)	μ^+ spectrum μ^+ spectrum & $R = 1.0 \pm 0.2$ $P^{\parallel}_{\mu} = +0.8^{+0.2}_{-0.8}$	(115-134)	122 50	$-27 \leq \xi \leq -7.6$ $\xi = -7.6$ in best agreement $\xi > -4$
8. J. Brown, et. al.[9] (12 in. Xe B. C.)	μ^+ & π^o spectra & angular correlations	($T_{\mu} = (12\text{-}85)$ effectively $T_{\pi^o} = (0\text{-}115)$)	76	$\xi = 1.8 \pm 1.6$
9. J. Dobbs, et. al.[11] (Filament Scintillating Chamber)	μ^+ spectrum μ^+ spectrum & $R = 1.0 \pm 0.2$	(50-124)	Approx. 104	$\xi \leq -2$, or $\xi \geq +5$ $\xi = -9$ (at 95% confidence level)
10. D. Cutts, et. al.[18] (Spark Chambers & Counters)	μ^+ spectrum & $P^{\parallel}_{\mu} = 0.61 \pm 0.39$	(107 - 126)	864 observed (489 after corrections)	Assuming ξ real, $\xi = 0.84 \pm 0.6$ Assuming ξ complex, $0.8 < \lvert \xi \rvert < 2.6$
11. G. Gidal, et. al.[19] (30 in. Berkeley B. C. Freon (C_3F_8)	$\langle P^{\parallel}_{\mu} \rangle = 0.74 \pm 0.16$	(38-96)	2988	$\xi = -0.15 \pm 0.90$ or $\xi = -4.05 \pm 0.75$
12. V. Smirnitski, et. al.[20] (Nuclear Emulsion)	$P^{\parallel}_{\mu} = 0.70 \pm 0.45$ & $R = 1.0 \pm 0.2$	(40-100)	309	$\xi = +2$ in best agreement
13. T. Groves, et. al. $K^-_{\mu 3}$ Decay in (30 in. Berkeley B. C. Propane & Freon)	μ^- spectrum & $R = 0.63 \pm 0.1$	(0-129)	138	$\xi = 0$ in best agreement

II. THEORY AND ITS APPLICATION IN ANALYSIS

The three-body leptonic decays of K^+ mesons:

$$K^+ \rightarrow \pi^o + L^+ + \nu, \quad (L \equiv \mu, e)$$

have experimentally been found to satisfy a pure vector coupling[9,15,36-38]. If we assume a vector coupling for the interaction, then the matrix element[5,39] for the decay process can be expressed as a product of (V-A) weak current[40,41] and a phenomenological strangeness non-conserving strong current:

$$M_{fi} = \left\langle \nu\, L^+\, \pi^o \middle| J^{\lambda}_{weak}\, J^{strong}_{\lambda} \middle| K^+ \right\rangle \tag{2.1}$$

$$= \left\langle \nu \middle| J^{\lambda}_{w} \middle| L \right\rangle \left\langle \pi \middle| J^{s}_{\lambda} \middle| K \right\rangle$$

where

$$\left\langle \nu \middle| J^{\lambda}_{w} \middle| L \right\rangle = \frac{G}{\sqrt{2}} \left[\bar{u}\,(p_\nu)\, \gamma_\lambda\, (1 + \gamma_5)\, v\,(p_L) \right]$$

u and v are spinors for the neutrino and lepton, and p_ν and p_L are their four-momenta, respectively. γ_λ and γ_5 are Dirac matrices; G = Weak Interaction constant.

Since the weak current contains the two component form of the neutrino wave function, $(1 + \gamma_5)\, v\,(p_\nu)$, one cannot distinguish physically between vector and axial vector couplings in the (V-A) contributions to the matrix element. The Feynmann diagram for the decay process is shown in Fig. 1, where the strong interaction contribution occurs in the box.

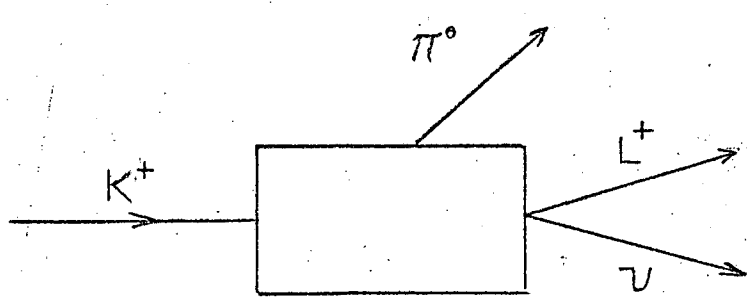

Fig. 1. Feynman diagram for $K^+_{\mu 3}$ decay.

In the approximation of local leptonic coupling, the lepton and the neutrino have a common origin, and only the sum of their momenta will be present in the matrix element. Then $\left\langle \pi \left| J_\lambda^s \right| K \right\rangle$ depends only on p_K and p_π, and may be written

$$\left\langle \pi \left| J_\lambda^s \right| K \right\rangle = \frac{1}{2(4E_K E_\pi)^{\frac{1}{2}}} \left(f_+ (q^2)\, Q_\lambda + f_- (q^2)\, q_\lambda \right), \quad (2.2)$$

where $$Q_\lambda \equiv (p_K + p_\pi)_\lambda ; \; q_\lambda \equiv (p_K - p_\pi),$$

and where E_K and E_π are the total energy of the K and the π, and the form factors $f_\pm$ are scalar functions of the invariant four-momentum transfer squared, $q^2 = (p_K - p_\pi)^2$. In the K^+ center-of-mass system, $\vec{p}_K = 0$, and $f_\pm$ are assumed to be slowly varying functions of the pion energy only,[4,39] and to a first approximation can be taken to be constant. If time reversal invariance is assumed to be valid, then f_+ and f_- are relatively real and can be taken as purely real numbers.

Evaluation of the square of the matrix element, where we have averaged over the spins of the leptons that are not observable in this experiment and integrated over the pion energies assuming the constancy of the form factors, yields the differential lepton energy spectrum for the K^+ decay at rest:[5]

$$d\Gamma_L = C' \, (E_L - m_L)^{\frac{1}{2}} \left\{ H_L \, (E_L) \right\} dE_L \qquad (\text{where } L \equiv \mu,\ e), \quad (2.3)$$

$$C' = \frac{1}{2\,(2\pi)^3\, M_K} \; . \quad (2.4)$$

To simplify the notation we specialize to the case where $L = \mu$:

$$H_\mu \, (E_\mu) = \frac{(\Delta - m_\pi^2 - 2M_K E_\mu)^2}{(\Delta - 2M_K E_\mu)} \left\{ f_+^2 \left[M_K E_\mu + \frac{1}{4} m_\mu^2 \left(\frac{M_K E_\mu - m_\mu^2}{\Delta - 2M_K E_\mu} \right) \right] + \right.$$
$$\left. + f_-^2 \frac{1}{4} m_\mu^2 \left(\frac{M_K E_\mu - m_\mu^2}{\Delta - 2M_K E_\mu} \right) + f_+ f_- \frac{1}{4} m_\mu^2 \left(\frac{2M_K^2 + m_\mu^2 - 3M_K E_\mu}{\Delta - 2M_K E_\mu} \right) \right\} , \quad (2.5)$$

with: $$\Delta \equiv M_K^2 + m_\mu^2 , \tag{2.6}$$

where: M_K and m_μ are the masses of the K and the μ, E_μ is the total energy of the muon, and f_+ and f_- are the form factors for the μ (the μ subscript is suppressed).

Equation (2.5) can be rewritten (see Appendix A) in terms of the ratio of the form factors:

$$\xi \equiv f_-/f_+ , \tag{2.7}$$

$$d\Gamma_\mu (E_\mu)/dE_\mu = C' f_+^2 \left[A(E_\mu) + \xi B(E_\mu) + \xi^2 C(E_\mu) \right] \tag{2.8}$$

If we interpret $(C' f_+^2)$ as a relative normalization constant, this equation then describes a one parameter theory characterized by ξ (see Fig. 2), which we later use in doing a χ^2 fit to the μ^+ spectral shape. Once the parameter is determined, then the curve is normalized to the number of $K^+_{\mu 3}$ events over the μ^+ energy region measured. The area under the entire spectral curve gives the total number of $K^+_{\mu 3}$ events. This number, in turn, is used in determining the $K^+_{\mu 3}$ branching ratio.

A relationship is now established, assuming μe-universality, between ξ and the ratio R of the total decay rates (or equivalently, the branching ratios) for the $K^+_{\mu 3}$ and $K^+_{e 3}$ decay modes.

The equation (2.8) can be integrated to give the total $K^+_{\mu 3}$ decay rate,

$$\Gamma_\mu^{TOT} = \int_{m_\mu}^{(E_\mu)_{MAX}} \left(\frac{d\Gamma_\mu (E_\mu)}{dE_\mu} \right) dE_\mu = (f_+)_\mu^2 \, (C_1 + C_2\xi + C_3\xi^2) \tag{2.9}$$

where: $C_1 = 5.66 \times 10^{13}$ (MeV)$^{9/2}$, $C_2 = 1.11 \times 10^{13}$ (MeV)$^{9/2}$, and $C_3 = 1.68 \times 10^{12}$ (MeV)$^{9/2}$.

An equation similar to (2.8) also holds for the $K^+_{e 3}$ decay mode. In this instance, however, the equation is simpler because the terms dependent on ξ and ξ^2 can be neglected because the smallness of the electron mass

and the fact that f_- and f_+ are of the same order of magnitude[5]. Integrating the equation over the electron energy gives:

$$\Gamma_e^{TOT} = \int_{m_e}^{(E_e)_{MAX}} \left(\frac{d\Gamma_e\ (E_e)}{dE_e} \right) dE_e = (f_+)_e^2\ C_4 \qquad (2.10)$$

where $C_4 = 8.76 \times 10^{13}\ (\text{MeV})^{9/2}$.

Dividing (2.9) by (2.10) and evaluating the constants gives:

$$R \equiv \frac{\Gamma_\mu^{TOT}}{\Gamma_e^{TOT}} = \left(\frac{f_{+(\mu)}}{f_{+(e)}} \right)^2 (0.646 + 0.126\ \xi + 0.0192\ \xi^2) \qquad (2.11)$$

with: $\xi = \dfrac{f_{-(\mu)}}{f_{+(\mu)}}$.

Replacing the total decay rates by branching ratios and noting that for μe-universality $(f_{+(\mu)}/f_{+(e)}) = 1$, then:

$$R = \frac{BR_{K_{\mu 3}}}{BR_{K_{e3}}} = (0.646 + 0.126\ \xi + 0.0192\ \xi^2). \qquad (2.12)$$

This equation is the expression that relates the K_{L3}^+ branching ratios to the parameter ξ. By utilizing existing experimental information on $BR_{K_{e3}}$ as input to (2.12), we then have a rather restrictive relationship between $BR_{K_{\mu 3}}$ and ξ. If we require that this relationship be compatible with the values of the $K_{\mu 3}^+$ branching ratio and form factor ratio, obtained from fitting the μ^+ spectrum and partial decay rate by using (2.8), we obtain much more restrictive limits on the values of $BR_{K_{\mu 3}}$ and ξ than can be obtained from (2.8) alone. This is discussed further in the analysis section and is illustrated in Fig. 17.

If time reversal invariance is not valid, then the form factors are relatively complex. But the entire formalism described is still valid with the substitutions[39].

$$\xi \rightarrow \mathrm{Re}\ \xi = \xi_{RE} \tag{2.13}$$

$$\xi^2 \rightarrow |\xi|^2 = \left[(\mathrm{Re}\ \xi)^2 + (\mathrm{Im}\ \xi)^2\right] = (\xi_{RE}^2 + \xi_{IM}^2) \tag{2.14}$$

where: $\mathrm{Re}\ \xi \equiv \xi_{RE}$, $\mathrm{Im}\ \xi \equiv \xi_{IM}$.

We have reanalyzed the data by using (2.8) with Re ξ and Im ξ as the two parameters to be determined in a maximum likelihood fit to the muon spectral shape. We also re-examined (2.12) in order to see what limits it imposes on Re ξ and Im ξ when one considers the experimental values and errors for $BR_{K_{\mu 3}}$ and $BR_{K_{e3}}$. We discuss the analysis procedures in detail in Section IV and display the results in Figs. 18 and 19.

III. EXPERIMENTAL PROCEDURE

A. The Exposure

In the summer of 1963, approximately 2.5×10^6 K^+ mesons were stopped in the Berkeley 30-inch heavy-liquid bubble chamber[42] filled with freon, C_3F_8. Under operating conditions the liquid has a density of 1.224 gm/cm^3 and a radiation length of 27 cm. The beam was designed so that most of the K^+ mesons stopped in a fiducial volume near the center of the chamber. However, the chamber was not large enough to contain all of the K^+ secondary decay products. One of the major difficulties of the experiment was that the probability of a μ^+ leaving the chamber was large and highly energy dependent. The longest μ^+ in $K^+_{\mu 3}$ decay is 46 cm, while the approximate visible fiducial volume of the chamber is 75 cm long x 45 cm wide x 30 cm in depth; the latter dimension is parallel to the chamber's surrounding magnetic field of mean value 15.2 kilogauss.

There were a total of about 2.5×10^5 three-view stereo pictures taken, with an average of ten stopping K^+ mesons per picture. These pictures were the first taken using the new scotchlight bright-field illumination technique[43], and were generally of good quality. Some sample K^+ decays are shown in Figs. 3 and 4; the pictures were selected to illustrate the different types of K^+ decay modes which were important in this experiment.

Tracks of particles in the bubble chamber photographs were identified from range, ionization and curvature. Electrons were also identifiable from Bremstrahlung and δ-rays. Stopping π^+'s were usually distinguishable from μ^+ by the characteristic $\pi\mu e$ decay chain on the end of the stopping pion.

B. The Beam

The beam transport equipment, designed by Goldhaber, et al.[44], provided a 750 MeV/c momentum-analyzed and velocity-separated beam of K^+ mesons (see Figs. 5 and 6) which were brought to rest in the Berkeley 30-inch heavy-liquid bubble chamber. The K^+ mesons were produced by protons impinging on a platinum target in one of the Bevatron straight sections. The secondary particles produced at 27.5° to the circulating proton beam, were allowed to enter the beam transport channel after passing through a collimator to limit the vertical acceptance. Momentum analysis took place at a bending magnet and momentum selection at the first mass slit. This collimator and the focusing properties of the bending magnets fringing field created a vertically parallel beam, which was passed through a ten-foot velocity spectrometer with a horizontal magnetic field and vertical electric field. The fields were adjusted so as to transmit the K^+ mesons undeflected. Pions and protons were deflected out of the median plane. All particles were focussed by a two-element quadrupole magnet on a collimating slit. The slit transmitted the K^+ mesons and stopped the secondary particles, which had been separated from the K^+ beam by the velocity spectrometer. The rest of the beam was a mirror image of what has been described so far, utilizing the K^+ image at the first focus as a source from which to form a final image at a second slit. There were approximately 10 K^+ mesons at the second slit per 10^{11} protons impinging on the target. Behind the second slit there was placed a saw-tooth shaped copper absorber which degraded and spread out the K^+ momenta so that the mesons could be brought to rest beyond the absorber within a rectangular-shaped region 5 inches wide by 10 inches long, centered vertically and horizontally inside the bubble chamber.

There was an attenuation factor of about two going through the absorber. Extra maneuverability of the K^+ beam was obtained by a small C magnet placed in front of the first slit.

In order to help separate the π^+ mesons from the K^+ beam, "separation curves" (see Fig. 7) were run at the second slit by tuning both spectrometers for K^+ mesons and then varying the magnetic field in one to sweep over a broad region around the best K^+ operating point.

C. Range-Energy Relations

The length of the stopping muon, L_μ, was a most convenient parameter, useful in establishing criteria for both scanning and analysis. We worked extensively with this variable and for reference have included in Appendix B a table of range-energy relations[45] for the muon and other particles. The range-energy relations were checked in three ways and found to hold within 1%. This was done by examining the range distribution of monoenergetic π^+ in $K^+_{\pi 2}$ decays and μ^+ in $K^+_{\mu 2}$ decays, and by checking the Q-value distribution of the K^+_τ decay. The Q-value was calculated by using the energies determined from measurements of the range of the outgoing pions in the K^+_τ decay.

D. Scanning

In order to obtain a sample of $K^+_{\mu 3}$ events as unbiased and background-free as possible, it was necessary to consider the effects of all of the K^+ decay modes. Table II lists the more common K^+ decays and some of their properties. (See also Figs. 3 and 4 for examples of K^+ decays.) We discuss some problems which led to the choice of the scanning criteria. The $K^+_{\mu 3}$ scan is complicated by the fact that $K^+_{\pi 2}$ and $K^+_{\tau'}$ decay modes

TABLE II. K^+ Decay Modes and Kinematical Data.

Ranges have been calculated; the other data is taken from Reference 23.

Decay Mode		Branching Ratio (%)	Range (cm)	Maximum Number of γ's	Momemtum in C.M. p^* (MeV/c)	C.M. Total Energy (MeV) $E^* = T^* + m\gamma^2$	Available K.E. in C.M. Q (MeV)
$(K\mu_3^+)$	$K^+ \rightarrow \pi^o + \mu^+ + \nu$	3.4 ± 0.32	$0 \leq L_\mu \leq 45.8$	2γ	$p^*_{MAX_\mu} = 215.3$ $p^*_{MAX_\pi} = 215.3$	$E^*_{MAX_\mu} = 239.8$ $E^*_{MAX_\pi} = 254.1$	253.2
(Ke_3^+)	$K^+ \rightarrow \pi^o + e^+ + \nu$	4.8 ± 0.32	$0 \leq L_e \leq M$ $M > 45.8$, but have Bremstrahlung	2γ	$p^*_{MAX_e} = 228.5$ $p^*_{MAX_\pi} = 288.5$	$E^*_{MAX_e} = 228.5$ $E^*_{MAX_\pi} = 265.4$	358.4
$(K\mu_2^+)$	$K^+ \rightarrow \mu^+ + \nu$	63.1 ± 0.8	$L_\mu = 54.3$	none	$p^* = 235.6$	$E^*_\mu = 258.3$	388.2
$(K\mu\gamma^+)$	$K^+ \rightarrow \mu^+ + \nu + \gamma$	--- *	$0 \leq L_\mu \leq 54.3$	1γ	$p^*_{MAX_\mu} = 235.6$	$E^*_{MAX_\mu} = 258.3$	388.2
$(K\pi_2^+)$	$K^+ \rightarrow \pi^+ + \pi^o$	21.5 ± 0.64	$L_\pi = 30.4$	2γ	$p^* = 205.3$	$E^* = 248.2$	219.3
(K_τ^+)	$K^+ \rightarrow \pi^+ + \pi^o + \pi^o$	1.7 ± 0.16	$0 \leq L_\pi \leq 10.1$	4γ	$p^*_{MAX_{\pi^o}} = 133.1$ $p^*_{MAX_{\pi^+}} = 132.3$	$E^*_{MAX_{\pi^+}} = 192.9$ $E^*_{MAX_{\pi^o}} = 189.0$	84.3
(K_τ^+)	$K^+ \rightarrow \pi^+ + \pi^+ + \pi^-$	5.5 ± 0.16	$0 \leq L_\pi \leq 8.6$	none	$p^*_{MAX_\pi} = 125.6$	$E^*_{MAX_\pi} = 187.8$	75.1

*By Calculation, $BR_{K\mu\gamma} \simeq \frac{BR_{K\mu_2}}{\alpha} = \frac{63.1\%}{137} = 0.461\%$, $\alpha \equiv$ Fine Structure Constant.

Radiative $K\pi_2^+$ decays are down by a factor of ≈ 3 from radiative $K\mu_2^+$ decays, and hence, are not significant.

Other known K^+ decay modes have branching ratios $\lesssim 1 \times 10^{-4}$ and are of no consequence for this paper.

look like $K^+_{\mu 3}$ events when their stopping π^+ secondary does not show the short μ^+ (having L_μ = 1.44 mm) in the characteristic $\pi\mu e$ chain. For the $K^+_{\tau'}$ mode (see Fig. 8) this decay sequence is:

$$K^+ \rightarrow \pi^+ + \pi^o + \pi^o$$
$$\hookrightarrow \mu^+ + \nu \quad , L_\mu = 1.44 \text{ mm}$$
$$\hookrightarrow e^+ + \nu + \bar{\nu}$$

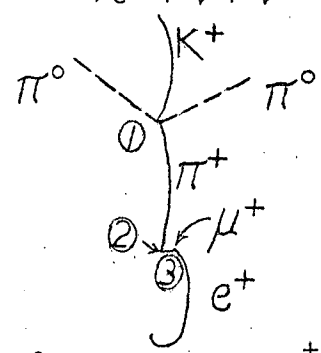

Fig. 8. Sketch of a $K^+_{\tau'}$ decay.

Another scanning difficulty resulted from the fact that the chamber was run in such a way that the last 3 cm of a stopping K^+ track were solid. Therefore, one could tell whether a K^+ meson had stopped before decaying only from looking at the ionization within the last 3 cm. This maximum residual range of 3 cm implies 2.5% of the K^+ decay in flight[46]. The only serious background introduced by the K^+ decay in flight was from the $K^+_{\mu 2}$ mode, when the μ^+ decays backwards in the K^+ center-of-mass system. A third difficulty is that there is appreciable multiple scattering in C_3F_8, particularly near the ends of stopping tracks, so that measurements of projected scattering angles or of projected decay-in-flight angles are limited to about 8°. or more.

In the scanning for $K^+_{\mu 3}$ events, an event was acceptable for the μ^+ spectrum and branching ratio determination whether or not it had any of the γ rays from the π^o decay converting in the chamber[47]. The $K^+_{\mu 3}$ scanning criteria adopted were:

1. To accept the events only when the K^+ decays appeared to be at rest.
2. To accept only events visible in all three views of the chamber.
3. To accept only events for which there were no μ^+ scatters with projected angle > 15°, unless the scatter occurred in the last cm.
4. To mark the event if there were any uncertainty about the existence of a $\pi\mu e$ decay chain at the end of the μ^+.

The last criterion was designed to speed decision making at the scan table and to find out how frequently these uncertain cases arose. They turned out to be a minor correction and were accounted for in the analysis. The scanners noted events having visible $\pi\mu e$ chains when the length of the track coming from the K^+ was greater than the maximum length of the π^+ from a $K^+_{\tau'}$ and less than the length of a π^+ from a $K^+_{\pi 2}$. This confirmed that background from K^+ decay in flight of the $K^+_{\tau'}$ and $K^+_{\pi 2}$ modes as well as possible shortening of the π^+ from small angle inelastic scattering in these decay modes, was negligible[48]. Also noted were possible $K^+_{\mu 3}$ events with short μ^+ ($L_\mu \leq 2$ cm) which might be confused with K^+_{e3} events in which the K^+ scatters near its end and the scatter is not obvious from ionization. The number of these events proved to be negligible, and in any case, were all eliminated in the final analysis which required all $K^+_{\mu 3}$ events to have $L_\mu \geq 3.0$ cm.

At the same time that the scanners were looking for $K^+_{\mu 3}$ events, they also looked for the easily recognized K^+_τ decays. The purpose of this was two-fold; first, to have a reference to known $\pi\mu e$ endings while scanning, and second, to record what fraction of the $\pi\mu e$ decay chains were not visible. We found (13 ± 3)% of the $\pi\mu e$ chains were not visible in scanning, where the error is an average estimated for all scanners

and for all the film scanned. This number was used in calculating the fraction of $K^+_{\pi 2}$ and $K^+_{\tau'}$ decays which contributed to the $K^+_{\mu 3}$ background.

In the experiment there were approximately 15,000 pictures scanned. From these pictures we measured 4,000 candidates, which after editing and analysis cuts and corrections were reduced to about 1000 $K^+_{\mu 3}$ events. All the candidates found in scanning were edited on the scan table in order to double check that they met the scan criteria and were good $K^+_{\mu 3}$ candidates. At the same time, each was checked to see that measured information on it had passed through the computer system and was ready for analysis. A portion of the computer output was checked by hand measurements on the scan table to make sure that it was correct.

A rescan of 20% of the film showed that the mean scan efficiency was (85 ± 3)%. There were biases detected for tracks with $L_\mu < 3$ cm, so only tracks with $L_\mu \geq 3$ cm were included in the spectrum. Also, in order to eliminate biases as a function of length for steep tracks, all events were restricted to lying within ± 37° of the chamber's horizontal plane. This corresponded to keeping only those events for which the μ^+ decayed within 60% of the total available 4π solid angle.

To make the $K^+_{\mu 3}$ branching ratio determination it was necessary to find the total number of stopping K^+ mesons in the experimental sample of $K^+_{\mu 3}$ film scanned. This number was obtained by normalizing to K^+_τ decays. In a separate scan from the $K^+_{\mu 3}$ scan, all of the K^+_τ decays at rest in the entire chamber were recorded. The same frames were scanned for K^+_τ events. The mean scan efficiency for finding the K^+_τ decays was 96%. We find that the total number of stopping K^+_τ decays in this experiment is 8560, a number calculated from the 8519 K^+_τ decays found and corrected by the (96 ± 2)% mean scan efficiency and by a 3.6% fiducial

volume factor which was determined by finding what percentage of K^+ origins lay outside of our defined fiducial volume.

E. Measuring and Data Processing

The particle tracks on the bubble chamber film were measured by making (X, Y) coordinate observations with digitized microscopes in all three stereo views at intermittent points along the track length. Computation consisted of spatial reconstruction of tracks, evaluation of momenta, angles, and error estimates, and calculation of derived quantities (e.g., energies, Q-values, etc.). This was done by the FOG-CLOUDY-FAIR data reduction system[49]. Of particular importance was the ability of the system to abstract, tabulate and output information in the form of lists, histograms, and magnetic tapes.

In the entire experiment we processed approximately 4000 candidates. The system, however, was not able to reconstruct L_μ, the muon length, of about one-third of these, namely, those tracks which curved more than 60° from the beginning of the track to its end. Generally these tracks were greater than 30 cm in length and included the high energy portion of the muon spectrum, ($30 < L_\mu < 46$ cm, corresponding to $100 < T_\mu < 134$ MeV), and $K_{\mu 2}$ decays (with $L_\mu = 54$ cm, used to check the range-energy relations). These long events were measured in two portions and their lengths reconstructed in programs written for this purpose.

It was convenient to handle much of our bookkeeping and analysis by producing IBM punched cards, one card for each event. Each card contained pertinent information which was used in analysis programs. Cards and lists on new events and remeasures were produced by merging the new information on a magnetic output tape from FAIR with the latest

magnetic tape in our analysis library. The new tape produced gave a cumulative total of all the events and information in the library.

IV. ANALYSIS

We discuss the analysis section in four parts. First, under the heading General Discussion, we present all the major features of the analysis, namely, the portion of the μ^+ spectrum studied, the nature of the background and biases, the geometrical corrections needed, and the general form of the χ^2 and maximum likelihood analysis functions. Then we outline our procedures under the headings Background Corrections, Geometrical Corrections, and Analysis Functions.

A. General Discussion

Initially, we hoped to measure the entire $K^+_{\mu 3}$ spectrum covering the μ^+ range $1.0 \leq L_\mu \leq 46$ cm corresponding to the μ^+ kinetic energy $12 \leq T_\mu \leq 134$ MeV (see Fig. 1). We found that because of scanning biases for short tracks that only the region with $L_\mu \geq 3$ cm could be studied. It was also found that because of large $K_{\pi 2}$ background at $L_\mu = 30.4$ cm, $T_\mu = 100$ MeV, we had to omit the region $28 < L_\mu < 33$ cm, $94 < T_\mu < 106$ MeV. Analysis of background in the high energy part of the spectrum $33 \leq L_\mu \leq 46$ cm, $106 \leq T_\mu \leq 134$ MeV, showed that the amount of background was the same within statistics as the number of observed events; hence, we gained no information from the high energy portion of the spectrum. This arose from high background corrections as well as small numbers of events resulting from the low detection efficiency for the higher energy μ^+ (see Table III). We were forced to omit the lower energy portion $3 \leq L_\mu < 8$ cm, $23 \leq T_\mu < 41$ MeV, because we felt the data was unreliable in this region due to large background and scanning biases for which it was difficult to make a precise correction (see Fig. 9).

In our final analysis we fitted the spectrum in the interval

$8 \leq L_\mu \leq 28$ cm, $41 \leq T_\mu \leq 94$ MeV. The same μ^+ spectral data used to determine ξ in the analysis of the K^+ decay mechanism was also used for the $K^+_{\mu 3}$ branching ratio determination and for the test of time reversal invariance.

The important background corrections in this experiment are listed below (see Fig. 9):

Background	Region of Importance L (cm)	Region of Importance T (MeV)	Contribution
(1) $K^+_{\tau'}$ ($\pi\mu e$ chain not visible)	(3 - 10),	(23 - 48)	12.1%
	(8 - 10),	(41 - 48)	4.4%
(2) $K^+_{\mu 2}$ (K^+ decays in flight)	(19 - 28),	(72 - 94)	7.8%
(3) (a) $K^+_{\pi 2}$ ($\pi\mu e$ chain not visible)	(28 - 33),	(94 - 106)	interval omitted
(b) $K^+_{\pi 2}$ (π^+ decays in flight)	(9 - 28),	(45 - 94)	4.6%
(4) $K^+_{\mu\gamma}$ (Radiative $K^+_{\mu 2}$ decay)	(3 - 28),	(23 - 94)	2.7%
	(8 - 28),	(41 - 94)	3.1%

We eliminate most of the $K^+_{\tau'}$ background when we measure the spectrum from (8 - 28) cm, omitting the region (3 - 8) cm. The percentage of $K^+_{\tau'}$ background over its region of contribution (3 - 10) cm drops from 12.1% to 4.4%. In omitting the region from (3 - 8) cm we lose very little sensitivity in fitting the data at the 95% confidence level as indicated from a χ^2 analysis, but we do eliminate most of our largest and least certain background correction and a region subject to scanning biases because of short μ^+ tracks. The percentage of $K^+_{\mu\gamma}$ background rises slightly from 2.7% of the data between (3 - 28) cm to 3.1% of the data between (8 - 28) cm. The percentage of $K^+_{\pi 2}$ (π^+ flt.) and $K^+_{\mu 2}$ (K^+ flt.) remains unchanged at 4.6% and 7.8% of their respective regions of contribution (9 - 28) cm and (19 - 28) cm (see Table IV). We note that the 4.6% $K^+_{\pi 2}$ (π^+ flt.) mode represents a partially corrected background, since the uncorrected contribuion was actually 10.1%. When the π^+ from

the $K^+_{\pi 2}$ mode decays in flight, the resultant track looks just like a μ^+ which scatters at a point corresponding to the $\pi\mu$ decay point, and which subsequently, decays into a positron. The large reduction was accomplished by calculating that most of these background events had the decay-in-flight space-angle, $\theta_{\pi\mu}$ (the angle between the π and the μ), in the interval $\theta_{\pi\mu} \geq 10°$, when $20 \leq (L_\pi + L_\mu) \leq 28$ cm. A careful scan table examination and kinematic fit of all $K^+_{\mu 3}$ events in the interval $20 \leq L_\mu \leq 28$ cm, eliminated 48 $K^+_{\pi 2}$ (π^+ flt.) background events. From calculations we expected 51.6 background events, in excellent agreement with experiment.

Geometrical corrections were important in studying the μ^+ spectrum because of the limited size of the chamber. Figures 14 and 15 show the probability of a track stopping in the chamber as a function of its total length. The experimental data was subjected to variations in the fiducial volume and to subdivision into ten equal increments of solid angle as a function of the polar angle θ (the angle between the μ^+ track and the z-axis). Invariance in shape of these differential distributions (corrected by Monte Carlo geometrical corrections) and plotted as a function of L_μ was a test for scanning biases. In order to eliminate biases as a function of length, we have restricted the data to be relatively flat by requiring that it lie within ± 37° of the horizontal plane. Even with this restriction, we found contamination from the only background mode of any significance which had an oriented angular dependence of the angle between the decay product and the incident direction of the decaying K^+ meson. This was the $K^+_{\mu 2}$ (K^+ flt.) mode. If the K^+ decays in flight and the μ^+ from the $K^+_{\mu 2}$ mode goes in the backwards direction, then the range of the decay particle will be shortened. Because of the large number of $K^+_{\mu 2}$ decays, the resulting shortened backward tracks create a significant background for tracks with $L_\mu \geq 19$ cm. We observed the experimental

range distribution of forward and backward decays and found the number in the backward direction larger by the expected number of $K^+_{\mu_2}$ (K^+ flt.) decays determined from a calculation. The calculation was made possible by the fact that the geometric correction factor was the same in the forward and backward directions. In effect, we neglected a special geometric correction for the $K^+_{\mu_2}$ (K^+ flt.) decay that would include correlations between the muon range and the angle between the K and the μ, and we found this approximation justifiable. Thus, we were able to use the same geometrical corrections for the $K^+_{\mu_2}$ (K^+ flt.) decay as we used for all the other K^+ decay modes.

In the data analysis we used the χ^2 and Maximum Likelihood methods to determine the value of the parameters which best fit the phenomenogical (V - A) theory which has been discussed in Section II. We take the point of view that a complete theory describes the data obtained by the experimenter. Since we have studied the μ^+ spectrum as a function of L_μ, the theory should predict the actual number of events as a function of L_μ, that were obtained under experimental conditions. Consequently, the theory of Section II must be modified to include geometrical and background corrections and scan efficiencies, and must be transformed from a function of T_μ to a function of R_μ, the range of the μ^+. Modifying the theory to make it a complete theory, rather than modifying the data to fit the incomplete theory, has the advantage that in complicated analysis functions the statistical factors are easily and properly handled. The χ^2 function is given by:

$$\chi^2 = \sum_{i=1}^{n} \left(\frac{N_{OBS_i} - N_{THY_i}}{\sigma_{THY_i}} \right)^2 \qquad (4.1)$$

where: $i = i^{\underline{th}}$ interval; n = Total number of intervals

N_{OBS_i} = Number of experimentally observed events in $i^{\underline{th}}$ interval

N_{THY_i} = Number of theoretically predicted events in $i^{\underline{th}}$ interval

σ_{THY_i} = Standard deviation of the ith interval.

In a random counting-type problem σ_{THY_i} is given by a Poisson distribution. When the statistics in the ith interval are equal to or greater than ten counts, the Poisson distribution in that interval can be approximated by a Normal or Gaussian distribution[50], and then $\sigma_{THY_i} = \sqrt{N_{THY_i}}$. For our problem we replace N_{THY_i} by the number for the modified theory, $N_{MOD\ THY_i}$, and then (4.1) becomes:

$$\chi^2(\xi) = \sum_{i=1}^{n} \left(\frac{N_{OBS_i} - N_{MOD\ THY_i}^{(\xi)}}{N_{MOD\ THY_i}^{(\xi)}} \right)^2 \tag{4.2}$$

The general form of $N_{MOD\ THY_i}$ is given in Table V, and the detailed structure of this variable is presented and discussed in the subsection on Analysis Functions. The procedure in the Chi-Squared test is to calculate $\chi^2(\xi)$ by varying the parameter ξ. The best fitting solution is obtained when ξ assumes the value which minimizes χ^2. Since we have constructed $N_{MOD\ THY}$ for the χ^2 function, the maximum likelihood function is easily obtained and is given by:

$$L(\xi) = \prod_{j=1}^{N_{OBS}^{TOT}} f(R_{\mu_j}, \xi) \tag{4.3}$$

$$f(R_{\mu_j}, \xi) = \frac{N_{MOD\ THY}(R_{\mu_j}, \xi)}{N_{OBS}^{TOT}} \tag{4.4}$$

where: j = the jth experimentally observed event

$N_{MOD\ THY}$ = Same modified theory function as for χ^2 in (4.2)

N_{OBS}^{TOT} = Total number of experimentally observed events

f = Probability function, normalized so that $\int f(R_\mu)\, dR_\mu = 1$

R_{μ_j} = Muon range measurement for the jth experimentally observed event.

TABLE III. Experimental Data and Background.†

(High energy part of μ^+ spectrum, $106 \leq T_\mu \leq 134$ MeV).

Closed-Open Interval (in cm)	R_μ(cm)	$N_{K\tau'}$	$N_{K\pi_2}$	$N_{K\mu_2}$	$N_{K\mu\gamma}$	N_{BKGD}	N_{OBS}
(28-33)	Data from entire region omitted because of $K\pi_2^+$ background.						
(33-34)	33.5	0.	4.73	2.86	1.00	8.59	11
(34-35)	34.5	0.	3.67	2.80	0.96	7.43	9
(35-36)	35.5	0.	2.87	2.47	0.89	6.23	3
(36-37)	36.5	0.	2.33	2.35	0.89	5.58	5
(37-38)	37.5	0.	1.76	2.10	0.85	4.71	4
(38-39)	38.5	0.	1.35	1.89	0.81	4.06	5
(39-40)	39.5	0.	1.01	1.76	0.76	3.54	2
(40-41)	40.5	0.	0.74	1.61	0.73	3.08	4
(41-42)	41.5	0.	0.54	1.37	0.69	2.60	0
(42-43)	42.5	0.	0.34	1.18	0.65	2.18	2
(43-46)	Has $N_{OBS} = 3$, and is omitted for lack of statistics.						

Interval Totals	$N^{TOT}_{K\tau'}$	$N^{TOT}_{K\pi_2}$	$N^{TOT}_{K\mu_2}$	$N^{TOT}_{K\mu\gamma}$	N^{TOT}_{BKGD}	N^{TOT}_{OBS}
(33-43)	0.	19.35	20.40	8.24	47.99	45

Since the number observed and the background calculated are the same within statistics, we can gain no information from the high energy portion of the spectrum.

†Symbols.

N stands for number, the subscripts indentify the variable.

R_μ= Mean range of μ^+ in a given interval; BKGD = Background;

OBS = Experimentally observed data, without corrections;

TOT = Total

TABLE IV. Experimental Data and Background.†

(Low and intermediate energy portion of μ^+ spectrum $23 \leq T_\mu \leq 94$ MeV).

Closed-Open Interval (in cm)	R_μ (cm)	$N_{K\tau'}$	$N_{K\pi_2}$	$N_{K\mu_2}$	$N_{K\mu\gamma}$	N_{BKGD}	N_{OBS}
(3-4)	3.50	15.62	0.	0.	1.22	16.85	74
(4-5)	4.50	12.88	0.	0.	1.23	14.11	67
(5-6)	5.50	10.24	0.	0.	1.24	11.49	79
(6-7)	6.50	7.63	0.	0.	1.28	8.91	51
(7-8)	7.50	5.53	0.	0.	1.30	6.83	72
(8-9)	8.50	4.18	0.	0.	1.31	5.48	69
(9-10)	9.50	1.85	0.17	0.	1.34	3.35	67
(10-11)	10.50	0.	0.65	0.	1.36	2.01	57
(11-12)	11.50	0.	1.52	0.	1.36	2.88	62
(12-13)	12.50	0.	2.11	0.	1.39	3.50	59
(13-14)	13.50	0.	2.52	0.	1.43	3.94	66
(14-15)	14.50	0.	3.29	0.	1.44	4.73	56
(15-16)	15.50	0.	3.81	0.	1.47	5.28	66
(16-17)	16.50	0.	4.22	0.	1.46	5.68	54
(17-18)	17.50	0.	4.91	0.	1.48	6.39	45
(18-19)	18.50	0.	5.21	0.	1.48	6.69	45
(19-20)	19.50	0.	5.81	0.08	1.48	7.37	47
(20-21)	20.50	0.	0.76	0.84	1.48	3.08	41
(21-22)	21.50	0.	0.65	1.66	1.44	3.74	37
(22-23)	22.50	0.	0.45	2.31	1.43	4.18	34
(23-24)	23.50	0.	0.38	2.70	1.40	4.49	23
(24-25)	24.50	0.	0.31	3.07	1.37	4.74	30
(25-26)	25.50	0.	0.33	3.22	1.33	4.88	20
(26-27)	26.50	0.	0.69	3.47	1.28	5.45	20
(27-28)	27.50	0.	1.12	3.58	1.25	5.95	16

Interval Totals	$N^{TOT}_{K\tau'}$	$N^{TOT}_{K\pi_2}$	$N^{TOT}_{K\mu_2}$	$N^{TOT}_{K\mu\gamma}$	N^{TOT}_{BKGD}	N^{TOT}_{OBS}	$N^{TOT}_{K\mu_3}$
(3-28)	57.93	38.90	20.91	34.25	151.99	1257	1105.01
(8-28)	6.02	38.90	20.91	27.97	93.80	914	820.20

†Symbols

N stands for number, the subscripts identify the variable

R_μ = Mean range of μ^+ in a given interval

BKGD = Background

OBS = Experimentally observed data, without corrections

TOT = Total

TABLE V. General Form of Analysis Functions

The purpose of this table is to display the general form of $N_{MOD\ THY_i}$, which is the main component of the χ^2 and maximum likelihood functions. By displaying $N_{MOD\ THY_i}$, one sees the use in the analysis functions of theory which gives $(d\Gamma/dE_\mu)$, range-energy relations which give (dT/dR), geometrical corrections which give F_{PPL_μ}, background corrections which give (dP/dT) and (dP/dR), and available empirical data such as branching ratios and scan efficiencies.

Definition of Symbols

N stands for number, the subscripts identify the variable.

R, T, E stand for range, kinetic energy, and total energy respectively.

OBS = Experimentally observed data, without corrections.

THY = Theory

MOD THY = Modified Theory

BKGD = Background

TOT = Total

BR = Branching Ratio

$\mu = \mu^+$ meson

dt = Increment in time

$\Gamma = K\mu_3^+$ muon decay rate

E_{ff} = Scan efficiency

F_{coul} = Probability for coulomb scattering at end of μ^+ in $K\mu_3^+$ decay.

$F_{PPL\mu_i}$ = μ^+ potential path length geometrical correction for the ith interval. (This was the same for the π^+, $F_{PPL\pi_i} = F_{PPL\mu_i}$)

P_k = Probability for contribution of Kth type of background.

F_{vol} = A fiducial volume correction factor, (see Section III C).

$(N_K)_{TOT}$ = Total number of K^+ mesons in experiment.

TABLE V. General Form of Analysis Functions

The χ^2 function is given by

$$\chi^2(\xi) = \sum_{i=1}^{n} \chi_i^2(\xi) = \sum_{i=1}^{n} \left[\frac{N_{OBS_i} - N_{MOD\ THY_i}^{(\xi)}}{\sqrt{N_{MOD\ THY_i}^{(\xi)}}} \right]^2 ,$$

where the number of modified theory events in the ith interval is

$$N_{MOD\ THY_i}^{(\xi)} = N_{THY_i}^{(\xi)} + N_{BKGD_i} .$$

Theory The number of theory events in the ith interval is given by

$$(N_{THY})_i = \left[\int_{\substack{\text{over} \\ i^{th}\text{ interval}}} \left(\frac{dN_{THY}}{dR_\mu}\right)_i (dR_\mu)_i \right] (F_{PPL_\mu})_i (E'_{ff})$$

N_{THY_i} is the number from theory corrected for geometry and efficiency over the ith interval.

The number per unit range can be expressed as a function of the number per unit energy

$$\left(\frac{dN_{THY}}{dR_\mu}\right)_i = \left(\frac{dN_{THY}}{dT_\mu}\right)_i \left(\frac{dT_\mu}{dR_\mu}\right)_i .$$

Background The number of background events in the ith interval is given by

$$N_{BKGD_i} = N_{K_{\tau'_i}} + N_{K_{\pi 2_i}} + N_{K_{\mu 2_i}} + N_{K_{\mu\gamma_i}} .$$

Let N_k be the kth type background mode. Then the kth type background in the ith interval is given by

$$(N_k)_i = \left[\int_{\substack{\text{over} \\ i^{th}\text{ interval}}} \left(\frac{dN_k}{dR}\right)_i (dR)_i \right] (F_{PPL_\mu})_i (E_{ff})$$

where $(N_k)_i$ is the number of kth background events corrected for geometry and efficiency.

The efficiency E'_{ff} is given by the scan efficiency E_{ff} for finding $K^+_{\mu 3}$ events, times the probability $(1 - F_{coul})$, that events were not accepted because the μ^+ scattered at its end (giving the muon the appearance of a pion background event with a $\pi\mu e$ decay chain). Thus

$$E'_{ff} = E_{ff}\,(1 - F_{coul}) \quad .$$

The number of events per unit energy (dN/dT_μ), is given by the $K^+_{\mu 3}$ decay rate per unit energy, $(d\Gamma/dE_\mu)$, integrated over unit time

$$\left(\frac{dN_{THY}}{dT_\mu}\right)_i = \left(\frac{dN_{THY}}{dE_\mu}\right)_i = \int_{\substack{\text{over}\\ i^{th}\text{ interval}}} \left(\frac{d\Gamma}{dE_\mu}\right)_i dt,$$

where we have transformed variables using

$$dT_\mu = dE_\mu, \text{ for } E_\mu = m_\mu c^2 + T_\mu \ .$$

The term $\left(\frac{d\Gamma}{dE_\mu}\right)_i$ is given by (2.8) in the theory section and has the form

$$\left(\frac{d\Gamma}{dE_\mu}\right)_i = K(\xi)\left[A(E_\mu) + B(E_\mu)\,\xi + C(E_\mu)\,\xi^2\right]$$

with, $\qquad K(\xi) = C'\,f_+^2,\ \xi = f_-/f_+ \ .$

For $N_{K_{\tau'}i}$ and $N_{K_{\mu\gamma}i}$ the number per unit range is expressed in terms of the number per unit energy

$$\left(\frac{dN_k}{dR}\right)_i = \left(\frac{dN_k}{dT}\right)_i \left(\frac{dT}{dR}\right)_i \quad ,$$

with the number per unit energy given by the product of $(N_K)_{TOT}$ the total number of K^+ mesons in the experiment, times BR_k and F_k, the branching ratio and the fractional contribution per unit energy, respectively, for the kth background mode

$$\left(\frac{dN_k}{dT}\right)_i = (N_K)_{TOT}\,(BR_k)\,(F_k)_i \quad .$$

Here, the total number of K^+ mesons is given by the total number of K^+_τ decays divided by the tau branching ratio, and corrected by F_{vol}, a small fiducial volume factor which estimates the number of taus lying outside the fiducial volume

$$(N_K)_{TOT} = \frac{(N_{K\tau})_{TOT}}{BR_{K\tau}}\,(1 - F_{vol}) \ ,$$

and the fractional contribution of the kth background mode per unit energy is given by the probability for its production per unit energy

$$(F_k)_i = \left(\frac{dP_k}{dT}\right)_i \quad .$$

For $N_{K_{\pi 2}i}$ and $N_{K_{\mu 2}i}$ two of the above expressions are modified, since these background contributions are calculated as a function of range rather than energy $\left(\frac{dN_k}{dR}\right)_i = (N_K)_{TOT}\,(BR_k)\,(F_k)_i$, and $(F_k)_i = \left(\frac{dP_k}{dR}\right)_i$.

We discuss the Likelihood Function in further detail in the subsection on Analysis Functions. We note that the procedure in the Maximum Likelihood test is to calculate L (ξ) by varying the parameter ξ. The best fitting solution is obtained when ξ assumes the value which maximizes L (ξ).

B. Background Corrections

We discuss the procedures used in making background corrections for the $K^+_{\tau'}$, $K^+_{\mu 2}$ (K^+ flt.), $K^+_{\pi 2}$ (π^+ flt.), and $K^+_{\mu\gamma}$ decay modes. The number of background events contributing to the observed data from the $k^{\underline{th}}$ background mode in the $i^{\underline{th}}$ interval has the general form (see Table V):

$$(N_k)_i^{TOT} = (N_k)_i^{TOT} \; (F_{PPL_\mu})_i \; (E_{ff})$$

$$(N_k)_i^{TOT} = \left\{ (F_k)_i \left[(N_K)_{TOT} \; (BR)_k \left(\begin{array}{c} \text{Transformation of} \\ \text{variable factor} \end{array} \right) \right] \right\} (F_{PPL_\mu})_i \; (E_{ff})$$

where: $(N_k)_i^{TOT}$ = Total amount of $k^{\underline{th}}$ type background produced in $i^{\underline{th}}$ interval.

$$\left(\begin{array}{c} \text{Transformation of} \\ \text{variable factor} \end{array} \right) = \begin{cases} \left(\frac{dT}{dR}\right)_i & \text{for } (N_{K_{\tau'}})_i;\ (N_{K\mu\gamma})_i \\ 1 & \text{for } (N_{K\pi 2})_i;\ (N_{K\mu 2})_i \end{cases}$$

The same geometric reduction factor, F_{PPL_μ}, and the same scan efficiency, E_{ff}, were used for all background modes. The branching ratio, $(BR)_k$, and the fractional contribution for each decay mode, F_k, vary for each type of contamination. For each background mode we have calculated $(F_k)_i$, the fractional contribution per unit interval (i).

$$(F_k)_i = \begin{cases} \left(\frac{dP_k}{dT}\right)_i & \text{for } (N_{K\tau'})_i;\ (N_{K\mu\gamma})_i \\ \left(\frac{dP_k}{dR}\right)_i & \text{for } (N_{K\pi 2})_i;\ (N_{K\mu 2})_i \end{cases}$$

where, for example: $\left(\frac{dP_k}{dT}\right)_i$ = the probability for contribution per unit kinetic energy in the $i^{\underline{th}}$ analysis interval, by the $k^{\underline{th}}$ background mode.

The corrections given in this section are collected together in Section Iv, D, on Analysis Functions.

1. $K^+_{\tau'}$ ($\pi\mu e$ chain not visible) Correction

The $K^+_{\tau'}$ background arises from $K^+_{\tau'}$ events which do not have a visible $\pi\mu e$ decay chain on the end of the π^+. The $\pi\mu e$ decay chain nondetection factor is $F_{\substack{no\\ \pi\mu e}} = (13 \pm 3)\%$. The $K^+_{\tau'}$ correction is made using the empirically determined π^+ spectrum in $K^+_{\tau'}$ decay[51]. The probability function for the $K^+_{\tau'}$, contribution per unit interval, is determined from the areas under the π^+ spectral curve by taking a ratio of the area within each interval to the area of the entire curve (see Fig. 10). We also take into account the fraction of π^+ mesons which interact in flight by multiplying the probability function by a π^+ absorption factor, $e^{-(x_i/\lambda_{C_3F_8})}$. The π^+ cross-section in C_3F_8 has been found to be consistent with geometric[52]. [illegible] Then the mean free path for nuclear interactions in C_3F_8 is $\lambda_{C_3F_8} = 58.5$ cm.

The total probability function is:

$$F_{K_{\tau'}} = \frac{\left(A_{K_{\tau'}}\right)_i}{\left(A_{K_{\tau'}}\right)_{TOT}} \left(e^{-x_i/\lambda_{C_3F_8}}\right) \left(F_{\substack{no\\ \pi\mu e}}\right)$$

where: $(A_{K_{\tau'}})_i$ = the area for the π^+ spectral curve, corresponding to the $i^{\underline{th}}$ interval

$(A_{K_{\tau'}})_{TOT}$ = total area under the π^+ spectral curve

$\left(e^{-x_i/\lambda_{C_3F_8}}\right)$ = π^+ absorption factor in the $i^{\underline{th}}$ interval

$(F_{\substack{no\\ \pi\mu e}})$ = $\pi\mu e$ decay chain non-detection factor.

2. $K^+_{\mu 2}$ (K^+ decay in flight) Correction

The $K^+_{\mu 2}$ (K^+ flt.) contamination arises because of the possibility that the K^+ decay has occurred within its last 3 cm of residual range. A 3 cm residual range corresponds to a maximum uncertainty in K^+ momentum of p_K = 215 MeV/c. This implies 2.5% of the K^+ mesons decay in flight.[46] The $K^+_{\mu 2}$ decaying at rest produces a monoenergetic μ^+ of momentum p_μ = 235.6 MeV/c. This momentum corresponds to L_μ = 54.3 cm, a length greater than the longest μ^+, with L_μ = 45.8 cm, in $K^+_{\mu 3}$ decay. If the K^+ decays in flight, then a μ^+ decaying backwards in the K^+ center-of-mass system can have its length sufficiently shortened in the laboratory system, depending on $\theta^*_{K\mu}$ (the center-of-mass angle between the K and the μ), that the length of the μ^+ in the laboratory system contaminates the $K^+_{\mu 3}$ spectrum for all $L_\mu \geq 19$ cm. This background is restricted in the K^+ center-of-mass system to $\theta^*_{K\mu} \geq 131°$. The corresponding restriction on the laboratory angle is $\theta_{K\mu} \geq 86°$.

We investigated the possibility of eliminating the $K^+_{\mu 2}$ (K^+ flt.) background events by constraining each $K^+_{\mu 3}$ event to the background hypothesis. For $K^+_{\mu 2}$ decays with the K^+ decaying in flight it is possible to calculate, from the muon momentum and the opening angle between the K^+ and the μ^+, the momentum of the incoming K^+ at the decay point. Since we know by ionization that the K^+ has a maximum residual range of 3 cm (corresponding to 215 MeV/c), most of the $K^+_{\mu 2}$ (K^+ flt.) background can be rejected as $K^+_{\mu 3}$ candidates. However, we have shown that if we use this as a selection criterion for eliminating the $K^+_{\mu 2}$ (K^+ flt.) background, we also eliminate a substantial number of genuine $K^+_{\mu 3}$ events. Therefore, we have approached the problem in a different fashion.

We wrote a computer program to calculate the probability function for the $K^+_{\mu 2}$ (K^+ flt.) background. The program divided the maximum residual K^+ laboratory momentum, p_K = 215 MeV/c, into 100 values corresponding to equal increments of probability for K^+ decay in flight. Because the K^+ decays isotropically in its center-of-mass system, the backward hemisphere in the center-of-mass could be divided into 100 increments of equal probability as a function of $\theta^*_{K\mu}$. Each of the values of p_K was combined by use of relativistic kinematics with the values of $\theta^*_{K\mu}$ to give in the laboratory system 10,000 sets of p_μ and $\theta_{K\mu}$. The program kept account of the probability for each of these decays, and after transforming $p_\mu \rightarrow L_\mu$, summed up the probabilities in 1-cm intervals. The results of the program are summarized for three values of the K^+ residual range in Fig. 11, where $F_{K\mu 2}$ (the background probability for $K^+_{\mu 2}$ (K^+ flt.) is plotted versus L_μ (the length of the muon).

3. $K^+_{\pi_2}$ (π^+ decay in flight) Correction

The $K^+_{\pi_2}$ (π^+ flt.) background correction arises because 4.0% of the π^+ mesons can decay in flight. Of these approximately 26% interact in flight before decaying. The remaining $\pi^+ \rightarrow \mu^+ + \nu$ decays are nearly all in the forward direction with approximately 93% of them having the angle between the π and the μ, $\theta_{\pi\mu}$, less than 21°. Consequently, our scan criterion of eliminating projected angles > 15°, corresponding to a mean space-angle of 21°, accepts essentially all of the π^+ decaying in flight. However, the K_{π_2} (π^+ flt.) mode is a background contamination for the spectrum only for lengths > 9 cm. It is most important over the measured spectrum in the region $20 \leq L_\mu \leq 28$ cm. In this region the major portion of the background was eliminated by using $K_{\pi 2}$ and $\pi\mu$ decay kinematics to discard $K_{\pi 2}$ (π^+ flt.) events with decay angles down to $\theta_{\pi\mu} = 10°$. Kinematics permitted separation of $K^+_{\pi_2}$ (π^+ flt.) events from $K^+_{\mu_3}$ events with a coulomb scatter.

A computer program was written to calculate the probability for a $K^+_{\pi_2}$ (π^+ flt.) event to be a background contribution. The program divided the π^+ momentum, p_π, into 100 values corresponding to equal increments of probability for π^+ decay in flight. The in flight π^+ nuclear interactions were taken into account by using a geometric absorption factor, $e^{-(x_i/\lambda_{C_3F_8})}$, the same as for the K^+_τ, background. [illegible] Assuming the μ^+ is emitted isotropically in the π^+ center-of-mass system, the 4π solid angle was divided into 100 increments of equal probability as a function of $\theta^*_{\pi\mu}$ (the angle between π and the μ in the π^+ center-of-mass system). Using relativistic kinematics, each of the values of p_π was coupled with a value of $\theta^*_{\pi\mu}$ to obtain p_μ

and $\theta_{\pi\mu}$ in the laboratory system. We converted $p_\mu \rightarrow L_\mu$ and $p_\pi \rightarrow L_\pi$, to find $L_{(\pi+\mu)} = (L_\pi + L_\mu)$, the total length of the π plus the μ. In the program we kept track of the probability for each event as a function of $L_{(\pi+\mu)}$ and $\theta_{\pi\mu}$. The results of the calculation are shown in Fig. 12 where we plot the background fraction contributed by the $K^+_{\pi 2}$ (π^+ flt.) mode, $F_{K_{\pi 2}}$, versus $L_{(\pi+\mu)}$, as a function of $\theta_{\pi\mu}$. In the analysis functions the curve labeled $\theta_{\pi\mu} = 21°$ was used for the region $8 \leq L_\mu \leq 20$ cm, while the $\theta_{\pi\mu} = 10°$ curve was used for the interval $20 \leq L_\mu \leq 28$ cm.

4. $K^+_{\mu\gamma}$ (Radiative $K_{\mu 2}$) Correction

The correction for $K^+ \rightarrow \mu^+ + \nu + \gamma$ was calculated using a modification in Cabibbo's theory[53] of radiative π^+ decay, $\pi^+ \rightarrow \mu^+ + \nu + \gamma$. Because of the similarity between the two decay modes, one can use the results of Cabibbo's radiative pion decay theory with the substitution of the K^+ mass for the π^+ mass, the substitution of $K^+_{\mu 2}$ and $K^+_{\mu\gamma}$ decay rates for the $\pi^+_{\mu 2}$ and $\pi^+_{\mu\gamma}$ decay rates, and the setting of R, a structure constant in $\pi^+_{\mu\gamma}$ decay, equal to zero[54]. The resulting final expression gives the $K^+_{\mu\gamma}$ decay rate as a function of the $K^+_{\mu 2}$ decay rate:

$$W_{K\mu\gamma}(E)dE = \left(\frac{e^2}{4\pi}\right) \frac{W_{K\mu 2}}{2\pi} \frac{1}{p_o^2} \left[(E_o - E)f(E) + \frac{4Ep_o}{E_o - E}\left(g(E) - \frac{p}{E}\right) \right] dE$$

where: $$f(E) = \ln\left[\frac{(E+p)M_K - m_\mu^2}{(E-p)M_K - m_\mu^2}\right]$$

$$g(E) = \ln\left[\frac{E+p}{m_\mu}\right]$$

$$p_o = \frac{(M_K^2 - m_\mu^2)}{2M_K} = \text{maximum momentum of } \mu$$

$$E_o = \frac{(M_K^2 + m_\mu^2)}{2M_K} = \text{maximum total energy of } \mu$$

M_K and m_μ are the rest masses of the K and the μ.

p and E are the momentum and total energy of the μ^+.

$W_{K\mu\gamma}$ and $W_{K\mu 2}$ are the $K^+_{\mu\gamma}$ and $K^+_{\mu 2}$ decay rates.

In Fig. 13 we plot $(W_{K\mu\gamma}/W_{K\mu_2})$ as a function of T_μ, the muon kinetic energy.

C. Geometrical Corrections

The most complicated correction in this experiment is the geometrical correction. Because of the limited size of the bubble chamber relative to the longest μ^+ in the spectrum, a large fraction of the muons from the $K^+_{\mu 3}$ decay escape detection by going outside of the chamber. The muons cannot be conclusively identified by ionization when they leave the chamber, but can be recognized when they stop in the chamber by the characteristic μe decay. Starting from the experimental number of $K^+_{\mu 3}$ decays found, in which the μ^+ decays in the chamber, one must be able to estimate the total number of decays that occurred. This has been made possible by a Monte Carlo computer program which generated randomly oriented decays, under the same experimental conditions which affect the potential path length of the actual decays. The purpose of the program was to obtain the potential path length distribution function, $F_{PPL\mu}(L_\mu)$. This function is dependent on the muon length, and is defined as the fraction of muons (with specified length, and generated from actual stopping K^+ origins) which stop within a given fiducial volume. The $F_{PPL\mu}(L_\mu)$ function is used to scale down the theoretically predicted μ^+ spectrum in the same way that the geometrical restrictions of both the chamber and the experimental conditions scale down the number of observable $K^+_{\mu 3}$ events, that have the μ^+ stopping in the fiducial volume.

If we did not have to make background and scan efficiency corrections, then the geometrical correction would be the only one needed in order to compare the theoretical predictions with the experimental observations.

We briefly state what the program did, and then discuss some pertinent details. The Monte Carlo program generated from experimental K^+ origins, randomly oriented μ^+ tracks of selected length, in successive 3 cm increments. The program incorporated range-energy relations, and averaged over each 3 cm segment of a generated track the effects of multiple scattering and magnetic curvature. It tabulated whether the propagated μ^+ track stopped within the chamber's specified fiducial volume or whether it went outside of this volume.

The μ^+ tracks were generated from a set of K^+ origins distributed throughout the film scanned and chosen in the following way. On a given frame every K^+ origin was measured, provided that the origin was visible in all three views and that the K^+ decayed at rest. The track coming from the K^+ did not necessarily have to stop in the chamber. A total of 560 stopping K^+ mesons and their decay origins were measured. The space angles θ and φ, defining the line of flight of the K^+ meson before decay, were determined from the measurements. Twenty of the 560 K^+ origins were found to lie outside of the outer-most fiducial volume. From each K^+ origin inside the fiducial volume were generated 20 identical sets of muon lengths. A set consisted of 20 different μ^+ lengths starting from 3 cm and increasing in 3 cm increments to 60 cm. Thus 20 muons of a given length, times 20 different lengths, gives 400 tracks generated from each origin. Since there were 540 useful K^+ origins, this meant we generated a total of 2.16×10^5 tracks. The program ran approximately 2-1/2 hours on the IBM-7094.

Each μ^+ meson was initially generated in a randomly oriented direction with respect to the line of flight of the decaying K^+ meson. Each track was propagated in successive 3 cm increments until it either stopped inside of the fiducial volume or went out of the fiducial volume. Both the tracks stopping within and going out the fiducial volume were separately tabulated as a function of L_μ, in ten equally probable increments of solid angle. The solid angle was taken as a function of the polar angle θ (the angle between the z-azis and the direction of the μ^+ track). The tracks were summed up in the 10 angular regions to give the outer fiducial volume corrections with no angular cuts (see Fig. 14). We also summed the tracks in the three angular regions on each side of the chamber's horizontal plane. This gave the fiducial volume correction for tracks lying within ± 37° of the horizontal plane. The ± 37° restriction corresponds to accepting μ^+ tracks lying within 60% of the 4π solid angle available in the chamber. The fiducial volume was varied by shrinking it 3 cm on all sides and running the program again. The potential path length distribution is sensitive to variations in the fiducial volume. In Fig. 15 is plotted the geometrical correction, $F_{PPL\mu}$, versus L_μ, for the outer and inner fiducial volumes when the tracks were restricted to lie within ± 37° of the chamber's horizontal plane. These curves represent the geometrical corrections used in the final analysis of the data.

D. Analysis Functions

The χ^2 function used to determine ξ and $BR_{K_{\mu 3}}$, and the maximum likelihood function used to test time reversal invariance by evaluating ξ_{RE} and ξ_{IM} have been introduced in (4.2), (4.3), (4.4) and Table V.

In this section we display the detailed form of these functions, tell how we normalize the theory and apply the χ^2 test to simultaneously determine ξ and $BR_{K_{\mu 3}}$, and we generalize (2.12), the relationship between $R = BR_{K_{\mu 3}}/BR_{K_{e3}}$ and ξ, by expressing R in terms of ξ_{RE} and ξ_{IM}.

The actual work of minimizing χ^2 and of maximizing the likelihood function was done in programs written in Fortran IV and run on the IBM-7044 computer. The programs printed out input data, did background calculations and displayed the results (as, e.g., in Tables III and IV), and normalized and evaluated the analysis functions, printing out appropriate results. Graphs of χ^2 versus ξ, and $BR_{K_{\mu 3}}$ versus ξ were drawn by using a CAL-COMP plotter.

The χ^2 Function

We bring together all the expressions used in the analysis of the data over the region $8 \leq L_\mu \leq 28$ cm. The data was analyzed by grouping the events into one cm increments (see Fig. 9). The component terms in the χ^2 function as given by (4.2) and Table V are now expressed as functions of T_μ and R_μ, and some quantities are evaluated. The definition of symbols is the same as in Table V.

$$\chi^2(\xi) = \sum_{i=8}^{n=28} \chi_i^2(\xi) = \sum_{i=8\,\mathrm{cm}}^{n=28\,\mathrm{cm}} \left(\frac{N_{OBS_i} - N_{MOD\,THY_i}^{(\xi)}}{\sqrt{N_{MOD\,THY_i}^{(\xi)}}} \right)^2 \qquad (4.5)$$

$$\text{where:} \quad N_{MOD\,THY_i}^{(\xi)} = N_{THY_i}^{(\xi)} + N_{BKGD_i} \qquad (4.6)$$

First we discuss the N_{BKGD_i} term

The background terms can be summarized using Table V and the expressions given in the section on Background Corrections.

$$N_{BKGD_i} = N_{K_{\tau'_i}} + N_{K_{\pi 2_i}} + N_{K_{\mu 2_i}} + N_{\mu\gamma_i}$$

In all the expressions below we have taken $(dR)_i \rightarrow (\Delta R)_i = 1$ for all intervals (i).

$$N_{K_{\tau'_i}} = \left[\frac{(A_{K_{\tau'}})_i}{(A_{K_{\tau'}})_{TOT}} \quad (e^{-x_i/\lambda} C_3 F_8)\ (F_{\substack{no\\ \pi\mu e}})\right] \left[(N_K)_{TOT}\ (BR_{K_{\tau'}})\ (\frac{dT_\pi}{dR_\pi})_i\right] (F_{PPL\mu})_i\ (E_{ff})$$

$$N_{K_{\mu 2_i}} = (F_{K_{\mu 2}})_i \left[(N_K)_{TOT}\ (BR_{K_{\mu 2}})\right] (F_{PPL\mu})_i\ (E_{ff})$$

$$N_{K_{\pi 2_i}} = (F_{K_{\pi 2}})_i \left[(N_K)_{TOT}\ (BR_{K_{\pi 2}})\right] (F_{PPL\mu})_i\ (E_{ff})$$

$$N_{K_{\mu\gamma_i}} = (\frac{W_{K_{\mu\gamma}}}{W_{K_{\mu 2}}})_i \left[(N_K)_{TOT}\ (BR_{K_{\mu 2}})\ (\frac{dT_\mu}{dR_\mu})_i\right] (F_{PPL\mu})_i\ (E_{ff})$$

where: $(N_K)_{TOT} = \frac{(N_{K_\tau})_{TOT}}{(BR_{K_\tau})}\ (1 - F_{vol})$

$$F_{\substack{no\\ \pi\mu e}} = 13\%,\ E_{ff} = 85\%,\ (N_{K_\tau})_{TOT} = 8560,\ F_{vol} = 20/560 = 3.6\%$$

The values of the Branching Ratios used appear in Table II.

<u>Next we discuss the N_{THY_i} term</u>

$$N_{THY_i}(\xi) = \int \left[\int (\frac{d\Gamma(\xi)}{dT_\mu})_i\ (dt)\ (\frac{dT_\mu}{dR_\mu})_i\right] (dR_\mu)_i \quad (F_{PPL\mu})_i\ (E'_{ff}) \tag{4.7}$$

$$N_{THY_i}(\xi) = \left[(\frac{dN_{THY}(\xi)}{dT_\mu})_i\ (\frac{dT_\mu}{dR_\mu})_i\right] (F_{PPL_\mu})_i\ (E'_{ff}) \tag{4.8}$$

where we have evaluated the integrals by taking: $dt \rightarrow \Delta t = 1$ sec

$$(dR_\mu)_i \rightarrow (\Delta R_\mu)_i = 1 \text{ cm for all intervals (i)}$$

we also have, $E'_{ff} = E(1 - F_{coul})$, $E = 85\%$, $F = 1.7\%$

and

$$(\frac{dN_{THY}(\xi)}{dT_\mu})_i = K(\xi) \left[A(T_\mu) + B(T_\mu)\xi + C(T_\mu)\xi^2\right]_i = K(\xi)\ G_i(\xi) \tag{4.9}$$

$$G_i(\xi) = \left[A(T_\mu) + B(T_\mu)\xi + C(T_\mu)\xi^2\right]_i$$

$K(\xi) = C' f_t^2$; $\xi = f_-/f_+$; A, B, C are given in Appendix A. Equation (4.9) has the same appearance as the expression for $(d\Gamma/dT_\mu)_i$, the rate per unit energy, however, (4.9) is simply the number per unit energy.

Normalization

Because the normalization was an important procedure in determining the $K^+_{\mu 3}$ branching ratio, we present a detailed discussion of the normalization. First, we elected to normalize $\left(\frac{dN_{THY}(\xi)}{dT_\mu}\right)$ to unity over the entire μ^+ spectrum for the 21 values of ξ, $\xi = -10, -9, \ldots, 0, \ldots, +9, +10$. Then (4.8) becomes:

$$N_{THY_i}^{(\xi)} = \left[\left(\frac{1}{A_{TOT}(\xi)}\right)\left(\frac{dN_{THY}(\xi)}{dT_\mu}\right)_i \left(\frac{dT_\mu}{dR_\mu}\right)_i\right] (F_{PPL_\mu})_i \, (E'_{ff})$$

where: $A_{TOT}(\xi)$ is the total area under the $\left(\frac{dN_{THY}(\xi)}{dT_\mu}\right)_i$

theoretical spectrum given by $G_i(\xi) = \left[A(T_\mu) + B(T_\mu)\xi + C(T_\mu)\xi^2\right]_i$

$N_{NTHY_i}^{(\xi)}$ is the normalized theory.

The normalization constant, $K(\xi)$, is a function of ξ, and is determined by the condition that the area under the $N_{NTHY}^{(\xi)}$ curve be equal over the part of the spectrum analyzed, to the actual number of $K^+_{\mu 3}$ events found (excluding background). Mathematically, this means:

$$\left(N^{OBS}_{K_{\mu 3}}\right)_{TOT} = \sum_{i=8\text{ cm}}^{n=28\text{ cm}} N_{NTHY}(\xi)_i = \sum_{i=8\text{ cm}}^{n=28\text{ cm}} \left[\left(\frac{1}{A_{TOT}(\xi)}\right)\left(\frac{dN_{THY}(\xi)}{dT_\mu}\right)_i \times \left(\frac{dT_\mu}{dR_\mu}\right)_i\right] (F_{PPL_\mu})_i \, (E'_{ff}) ,$$

$$\left(N^{OBS}_{K_{\mu 3}}\right)_{TOT} = K(\xi) \sum_{i=8}^{28} \left[\frac{G_i(\xi)\left(\frac{dT_\mu}{dR_\mu}\right)_i}{A_{TOT}(\xi)} (F_{PPL_\mu})_i\right] (E'_{ff}) , \qquad (4.10)$$

where: $(N^{OBS}_{K_{\mu 3}})_{TOT} = \sum_{i=8cm}^{n=28cm} \left[(N_{OBS})_i - (N_{BDGD})_i \right]$

$$G_i(\xi) = \left[A(T_\mu) + B(T_\mu)\,\xi + C\,(T_\mu)\,\xi^2 \right]_i .$$

The normalization constant, $K(\xi)$, is determined when (4.10) is solved for $K(\xi)$ and all operations carried out. In (4.10), the following interpretation holds for the three terms on the right hand side of the equation.

$K(\xi)$ = Total number of $K^+_{\mu 3}$ events in the experiment (over the entire μ^+ spectrum).

$$\sum_{i=8cm}^{28cm} \left[\frac{G_i(\xi)\,\left(\frac{dT_\mu}{dR_\mu}\right)_i}{A_{TOT}(\xi)} \quad (F_{PPL_\mu})_i \right]$$ = Fraction of the total μ^+ spectrum measured, but scaled down for the geometry limitations of the chamber.

E'_{ff} = Efficiency for detection of actual $K^+_{\mu 3}$ events.

<u>Determination of ξ and the $K^+_{\mu 3}$ Branching Ratio</u>

The experimental $K^+_{\mu 3}$ branching ratio is given by:

$$BR_{K_{\mu 3}}(\xi) = \frac{K(\xi)}{(N_K)_{TOT}} = \frac{\left[\begin{array}{l}\text{Total number of } K^+_{\mu 3} \text{ events}\\ \text{in entire spectrum}\end{array}\right]}{\left[\begin{array}{l}\text{Total number of } K^+ \text{ mesons}\\ \text{in the experiment}\end{array}\right]} \qquad (4.11)$$

This is an experimental determination of the branching ratio because we have normalized to the number of observed $K^+_{\mu 3}$ events. A different value of $BR_{K_{\mu 3}}$ is obtained for each value of ξ, since each theoretical ξ-curve encloses a different amount of area. Each area corresponds to different numbers of $K^+_{\mu 3}$ events over the entire μ^+ spectral shape, and hence, gives different values of $K(\xi)$ in (4.11). When we do a χ^2 fit to the μ^+ spectral shape using (4.5), we obtain some value of ξ which minimizes χ^2. This is interpreted statistically as the value of ξ which best fits

the hypothesis. We can select as the best value of the $K^+_{\mu 3}$ branching ratio that measurement which corresponds to the same value of ξ which minimizes χ^2.

There is another method for simultaneously determining ξ and the $K^+_{\mu 3}$ branching ratio. This involves plotting $BR_{K_{\mu 3}}$ versus ξ using (4.11) and (2.12). The intersection of the curves determines two sets of solutions for ξ and $BR_{K_{\mu 3}}$. One of these can be ruled out by using the χ^2 test to show that the value of ξ obtained is extremely unlikely. The results of applying this method are presented in the next section.

Maximum Likelihood Function

We generalize the likelihood function given in (4.3) and (4.4) by expressing it as a function of two parameters, ξ_{RE} and ξ_{IM}. This is done by first recalling (4.3) and (4.4),

$$L(\xi) = \prod_{j=1}^{N^{TOT}_{OBS}} f(R_{\mu_j}, \xi)$$

$$f(R_{\mu_j}, \xi) = \frac{N_{MOD\ THY}(R_{\mu_j}, \xi)}{N^{TOT}_{OBS}} ,$$

and noticing from (4.6) and (4.8) that $N_{MOD\ THY_i}$ depends on N_{THY_i}, and hence on the theoretical μ^+ spectrum (4.9):

$$\frac{dN_{THY}(\xi)}{dT_\mu} = K(\xi) \left[A(T_\mu) + B(T_\mu)\, \xi + C(T_\mu)\, \xi^2 \right] .$$

If we substitute into the above equation the expressions (2.13) and (2.14),

$$\xi \rightarrow \mathrm{Re}\ \xi = \xi_{RE},$$

$$\xi^2 \rightarrow |\xi|^2 = \left[(\mathrm{Re}\ \xi)^2 + (\mathrm{Im}\ \xi)^2 \right] = (\xi^2_{RE} + \xi^2_{IM}) ,$$

where $\mathrm{Re}\ \xi = \xi_{RE}$, $\mathrm{Im}\ \xi = \xi_{IM}$,

we can obtain the generalized likelihood function,

$$L\ (\xi_{RE},\ \xi_{IM}) = \prod_{j=1}^{N_{OBS}^{TOT}} f(R_{\mu j};\ \xi_{RE},\ \xi_{IM})\ , \tag{4.12}$$

$$f(R_{\mu j};\ \xi_{RE},\ \xi_{IM}) = \frac{N_{MOD\ THY}\ (R_{\mu j};\ \xi_{RE},\ \xi_{IM})}{N_{OBS}^{TOT}} \tag{4.13}$$

The generalized likelihood function is calculated by selecting fixed values of ξ_{RE} and ξ_{IM}, and then evaluating the normalized probability function f for each event in the observed data. The values obtained for given ξ_{RE} and ξ_{IM} are all multiplied together to give a single value for the likelihood function. Since the likelihood function depends on the parameter ξ_{IM} only in the form of ξ_{IM}^2, we can determine the magnitude of ξ_{IM}, but not its sign. By evaluating a sufficient number of points we determine a likelihood surface as a function of ξ_{RE} and ξ_{IM}. The maximum value on the surface determines the most likely solutions for ξ_{RE} and ξ_{IM}. We evaluated the likelihood function for ξ_{RE} and ξ_{IM} in 1/4 increments over the intervals

$$\xi_{RE} = -5,\ -4\tfrac{3}{4},\ \ldots,\ 0,\ \ldots,\ +4\tfrac{3}{4},\ +5,$$
$$\xi_{IM} = 0,\ \tfrac{1}{4},\ \tfrac{2}{4},\ \ldots,\ +4\ .$$

The results of the analysis are presented in Section V.

<u>The Ratio $R = \frac{BR_{K_{\mu 3}}}{BR_{K_{e3}}}$ and Constraints on ξ_{RE} and ξ_{IM}</u>

If the substitutions $\xi \rightarrow \xi_{RE}$

and $\xi^2 \rightarrow (\xi_{RE}^2 + \xi_{IM}^2)$

are made in (2.12), $R = \frac{BR_{K_{\mu 3}}}{BR_{K_{e3}}} = (0.646 + 0.126\ \xi + 0.0192\ \xi^2)$,

then the equation is transformed into the equation of a circle in the complex ξ-plane.

Let $c_1 = 0.646,\ c_2 = 0.126,\ c_3 = 0.0192$

then $$\xi_{RE}^2 + \xi_{IM}^2 + \left(\frac{c_2}{c_3}\right) \xi_{RE} + \left(\frac{c_1 - R}{c_3}\right) = 0$$

This is the equation of a circle with

Center at $$\left[\xi_{RE} = -1/2 \left(\frac{c_2}{c_3}\right),\ \xi_{IM} = 0\right] \rightarrow (-3.28,\ 0) \qquad (4.14)$$

and Radius $$|\xi| = 1/2 \left[\left(\frac{c_2}{c_3}\right)^2 - 4\left(\frac{c_1 - R}{c_3}\right)\right]^{1/2} \qquad (4.15)$$

The next section gives the results of evaluating (4.15) for ξ_{RE} and ξ_{IM}, using the value of R based on the average published value of the K^+_{e3} branching ratio and our measured value of the $K^+_{\mu 3}$ branching ratio.

V. RESULTS

We have determined ξ and the $K^+_{\mu 3}$ branching ratio by fitting the μ^+ kinetic energy spectrum and absolute rate over the region $41 \leq T_\mu \leq 94$ MeV, with 914 observed events (see Fig. 9). After background corrections were made this number was reduced to 820 actual $K^+_{\mu 3}$ events. The results of fitting the data with a χ^2 test of hypothesis for a one parameter (V - A) theory, yields, when χ^2 is a minimum, $\xi = 0\ ^{+2.0}_{-1.4}$, where the error corresponds to going up one unit in χ^2 from the point where χ^2 is a minimum. Using the above value of ξ, we find the $K^+_{\mu 3}$ branching ratio is $BR_{K_{\mu 3}} = (2.93 \pm 0.23)\%$. These values of ξ and $BR_{K_{\mu 3}}$ represent an excellent fit, for $\chi^2_{MIN} = 11.3$ with 18 degrees of freedom. This low value of χ^2 corresponds to a 15% confidence level and is due to the statistically excellent fit of the data and not due to overestimation of the errors. The χ^2 function was calculated for 21 integral values of ξ from -10 to +10. Figure 16 shows a plot of the χ^2 distribution as a function of ξ. A scan efficiency of 85% and 13% correction for nondetection of $\pi\mu e$ chains was used. The solutions are insensitive to variations in the scan efficiency by ±5%, and to ±3% variations in the $\pi\mu e$ chain nondetection factor, $F_{\substack{no \\ \pi\mu e}} = (13 \pm 3)\%$. Modification of the μ^+ theoretical spectral curves to include straggling indicates that this effect is completely negligible. At the 95% confidence level, where $\chi^2 = 29$ for 18 degrees of freedom, all values of ξ from -4.0 to +10.0 (the highest value tested) are possible. The experimental $K^+_{\mu 3}$ branching ratio, from (4.11), is shown in Fig. 17 to be rather insensitive to variations in ξ, and over the range $-4.0 \leq \xi \leq +10.0$ assumes the values $2.88 \leq BR_{K_{\mu 3}} \leq 3.09\%$. (The curves on each side of the middle curve are determined from a calculated 8% error on $BR_{K_{\mu 3}}$.)

As discussed in Section IV, D, on Analysis Functions, we can assume μe-universality and the value of the K^+_{e3} branching ratio, BR_{Ke3} = $(4.8 \pm 0.32)\%$,[23] to calculate a set of $K^+_{\mu 3}$ branching ratio curves which are a function of ξ. These are plotted in Fig. 17, and intersect the experimentally determined $K^+_{\mu 3}$ branching ratio curves of (4.11) in two regions. We can exclude the solution with ξ more negative than -4.5 to better than a 99% confidence level. This leaves the simultaneous solutions $\xi = -0.4 \pm 0.9$ and $BR_{K_{\mu 3}} = (2.9 \pm 0.3)\%$, which are consistent with the values obtained from minimizing χ^2 in the one parameter fit.

The same spectral data was analyzed by using the Maximum Likelihood Method to determine ξ_{RE} and ξ_{IM}. Since the likelihood function contains ξ_{IM} only in the form ξ^2_{IM}, it is symmetric with respect to reflections about the ξ_{RE} axis. Consequently, we can determine only the magnitude of ξ_{IM} and not its sign. The likelihood function was calculated for values of ξ_{RE} and ξ_{IM} in intervals of 1/4 over the range

$$\xi_{RE} = -5, -4\tfrac{3}{4}, \ldots, 0, \ldots, +4\tfrac{3}{4}, +5,$$
$$\xi_{IM} = 0, \tfrac{1}{4}, \tfrac{1}{2}, \ldots, +4.$$

The most likely solution occurs when $\xi_{RE} = \xi_{IM} = 0$, where the likelihood function is a maximum. Because the likelihood function is non-Gaussian, a simple confidence interval interpretation is ruled out. Figure 18 shows the projection of the likelihood function onto the complex ξ-plane. To examine the sensitivity of the solution we have plotted in Fig. 18 the projected $e^{-0.5}\, L_{MAX}$ and $e^{-2.0}\, L_{MAX}$ contours of the likelihood function, corresponding to the one and two standard deviation levels of a Gaussian distribution.

For $L(\xi_{RE}, \xi_{IM}) = e^{-0.5}\, L_{MAX}$, $\xi_{RE} = 0^{+1.6}_{-1.2}$, and $\xi_{IM} = 0 \pm 1.4$;

$L(\xi_{RE}, \xi_{IM}) = e^{-2.0}\, L_{MAX}$, $\xi_{RE} = 0^{+3.6}_{-2.1}$, and $\xi_{IM} = 0 \pm 2.9$.

These solutions are consistent with the results of the one parameter χ^2 analysis.

Finally, using (4.14) and (4.15), we compute the values of ξ_{RE} and ξ_{IM} from the ratio $R = BR_{K_{\mu 3}}/BR_{K_{e3}}$. We use our value for the $K^+_{\mu 3}$ branching ratio, $BR_{K_{\mu 3}} = (2.9 \pm 0.3)\%$, and the average value for the K^+_{e3} branching ratio, $BR_{K_{e3}} = (4.8 \pm 0.32)\%$,[23] to obtain $R = (0.60 \pm 0.074)$. This value of R gives a circle in the complex ξ-plane, with center at ($\xi_{RE} = -3.28$, $\xi_{IM} = 0$), and radius $|\xi| = 2.93^{+0.60}_{-0.76}$ (see Fig. 19). The intersections on the real axis, where $\xi_{IM} = 0$ are $-1.1 \leq \xi_{RE} \leq 0.25$ and $-6.8 \leq \xi_{RE} \leq -5.4$. Of these two solutions, the second solution is ruled out, since it is less than 10^{-6} times as likely as the value of ξ_{RE} corresponding to the peak value of the maximum likelihood solution. The first solution is compatible with the results of the χ^2 and maximum likelihood analysis.

We summarize and interpret our results in the Conclusion which follows this section.

VI. CONCLUSION

When we fit the μ^+ spectral data with a one parameter (V - A) theory, we find that the best solution for the purely real or purely imaginary parameter $\xi = f_-/f_+$, occurs when $\xi = 0^{+2.0}_{-1.4}$ at the point where χ^2 is a minimum. Using the above value of ξ, we find the corresponding value of the $K^+_{\mu 3}$ branching ratio is $BR_{K_{\mu 3}} = (2.93 \pm 0.23)\%$. These values of ξ and $BR_{K_{\mu 3}}$ represent the best statistical estimate in this experiment of the true values of these parameters. A determination of the values of ξ which are compatible with the data shows that at the 95% confidence level all values of ξ from -4.0 to +10.0 (the highest value tested) are possible. The $K^+_{\mu 3}$ branching ratio is rather insensitive to variations in ξ, and over the range -4.0 to +10 assumes the values $2.88 \leq BR_{K_{\mu 3}} \leq 3.09\%$. However, if we assume μe-universality and use the experimental value of the K^+_{e3} branching ratio, $BR_{K_{e3}} = (4.8 \pm 0.32)\%$,[23] we can simultaneously determine rather restricted values for ξ and the $K^+_{\mu 3}$ branching ratio. These are $\xi = -0.4 \pm 0.9$ and $BR_{K_{\mu 3}} = (2.9 \pm 0.3)\%$. On the basis of this solution we can reject those theories that predict $|\xi|$ is large--for example, the theory of Schwinger[8]--but we cannot discriminate among those theories which assume a K^+ decay mechanism that predicts ξ near zero. These include $K\pi$ resonance models,[3,6] $K\pi$ S- and P-wave scattering models,[4,7] and theories involving an intermediate vector boson[5].

If we assume that ξ is complex and do a two parameter maximum likelihood fit to the spectral data in order to determine ξ_{RE} and ξ_{IM}, we find that the likelihood function is a maximum when ξ_{RE} and $\xi_{IM} = 0$. This solution is consistent with the results of the one parameter χ^2 analysis. The likelihood function is non-Gaussian, hence, a simple

confidence interval interpretation is ruled out. Its sensitivity can be indicated by quoting the parameter values corresponding to $e^{-0.5}$ and $e^{-2.0}$ of the maximum value of the likelihood functions:

For $L(\xi_{RE}, \xi_{IM}) = e^{-0.5} L_{MAX}$, $\xi_{RE} = 0^{+1.6}_{-1.2}$, and $\xi_{IM} = 0 \pm 1.4$;

$L(\xi_{RE}, \xi_{IM}) = e^{-2.0} L_{MAX}$, $\xi_{RE} = 0^{+3.6}_{-2.1}$, and $\xi_{IM} = 0 \pm 2.9$.

Because Cabibbo's theory[30] calls for a violation of time-reversal invariance in $K^+_{\mu 3}$ decay but does not specify the magnitude of the violation, it is difficult to know whether these results have the precision to exclude his theory. The data gives a best fit maximum likelihood solution which is consistent with the time-reversal invariance requirement that $\xi_{IM} = 0$. This solution supports those theories[25-29] which call for no violation of time reversal invariance in $K^+_{\mu 3}$ decay.

ACKNOWLEDGMENTS

The author wishes to acknowledge and extend special thanks to Professor Wilson M. Powell for his help and support of this work. Insight into many of the problems and methods of experimental high energy physics has been gained from his collaboration.

Dr. George Kalmus, who has studied K^+ decays, was immensely helpful in many ways and always available for profitable discussions.

Dr. Robert P. Ely, Jr. has contributed greatly to my understanding an application of statistics to problems of analysis and, in general, to critical scientific thinking.

Dr. Robert W. Birge and Dr. George Gidal have made most useful suggestions and have been available for illiminating discussions.

Thanks are due to Professor George Saphir for help in scanning and for encouraging discussions during the initial phases of this experiment.

The help and co-operation in scanning, measuring and processing data was a contribution by many members of the data processing section of the Powell-Birge group under Mr. Wes Weber and of the Data Handling Group headed by Mr. Howard S. White. In particular, Mrs. Rho Gamow did much of the scanning.

Warm appreciation is extended to Mr. Edward Strasbourger, who helped with programming and analysis, and to Mr. Loren Shalz, whose patience and help were indispensible in obtaining information from the FOG-CLOUDY-FAIR system.

Drs. Warner Hirsch, Peter Newcomb, William J. Singleton, Yu-Li Pan and Thomas G. Schumann have all participated, at various times, in discussions which have clarified many ideas.

The author is grateful to Mrs. Kathy Pierce for help in typing this manuscript.

Other people in our group and in other groups at the Berkeley Radiation Laboratory have given generous assistance in time of need. To all of these people, my sincere thanks.

This work was done under auspices of the U. S. Atomic Energy Commission.

REFERENCES

1. A. Pais, Weak Interactions, The Quantum Theory of Fields, Proceedings of the Twelfth Conference on Physics at the University of Brussels, October 1961, Edited by R. Stoops (Interscience, New York, 1962), p. 101.

2. L. B. Okun, in Proceedings of the International Conference on High-Energy Nuclear Physics, Geneva, 1962 (CERN Scientific Information Service, Geneva, Switzerland, 1962), p. 843.

3. S. Oneda, Nucl. Phys. 57, 89 (1964).

4. H. Chew, Phys. Rev. Letters 8, 297 (1962).

5. N. Brene, L. Egardt, and B. Qvist, Nucl. Phys. 22, 553 (1961).

6. J. Bernstein and S. Weinberg, Phys. Rev. Letters 5, 481 (1960).

7. S. W. MacDowell, Phys. Rev. 116, 1047 (1959).

8. J. Schwinger, Phys. Rev. Letters 12, 630 (1964).

9. J. L. Brown, J. A. Kadyk, G. H. Trilling, R. T. Van de Walle, B. P. Roe, and D. Sinclair, Phys. Rev. Letters 8, 450 (1962); also see J. L. Brown, J. A. Kadyk, G. H. Trilling, R. T. Van de Walle, B. P. Roe, and D. Sinclair, in International Conference on High-Energy Nuclear Physics, Geneva, 1962 (CERN Scientific Information Service, Geneva, Switzerland, 1962), p. 462;
J. L. Brown, J. A. Kadyk, G. H. Trilling, R. T. Van de Walle, B. P. Roe, and D. Sinclair, Experimental Analysis of Ke_3 and $K\mu_3$ Decay, Lawrence Radiation Laboratory Report UCRL-10205, June 1962 (unpublished).

10. A. M. Boyarski, E. C. Loh, L. Q. Niemela, D. M Ritson, R. Weinstein, and S. Ozaki, Phys. Rev. 128, 2398 (1962).

11. J. M. Dobbs, K. Lande, A. K. Mann, K. Reibel, F. J. Sciulli, H. Uto, D. H. White, and K. K. Young, Phys. Rev. Letters 8, 295 (1962).

12. G. Zweig, Phys. Rev. 130, 2449 (1963).

13. C. L. Sandler and W. M. Powell, Bull. Am. Phys. Soc. 9, 722 (1964).

14. G. Gidal, W. M. Powell, R. T. Pu, C. L. Sandler, U. Camerini, W. F. Fry, R. Hantman, R. March, D. Murphree, and S. Natali, Lawrence Radiation Laboratory Report UCRL-11547, July 1964 (paper submitted to the 1964 International Conference on High Energy Physics, Dubna, U.S.S.R., August 1964).

15. G. L. Jensen, F. S. Shaklee, B. P. Roe, and D. Sinclair, Phys. Rev. 136, B 1431 (1964);
also see G. L. Jensen, B. P. Roe, D. Sinclair, and F. S. Shaklee, Bull. Am. Phys. Soc. 9, 34 (1964);
G. L. Jensen, Study of the Three-Body Leptonic Decay Modes of the K^+ Meson (Ph.D. Thesis), University of Michigan, 1964 (unpublished).

16. G. Giacomelli, D. Monti, G. Quareni, A. Quareni-Vigudelli, W. Püschel and J. Tietge, Nuovo Cimento 34, 6182 (1964).

17. V. Bisi, G. Borreani, R. Cester, A. De Benedetti, M. I. Ferrero, C. M. Garelli, A. Marzari-Chiesa, B. Quassiati, G. Rinaudo, M. Vigone, and A. E. Werbrouck, Phys. Rev. Letters 12, 490 (1964);
and erratum, ibid. 12, 656 (1964);
see also V. Bisi, G. Borreani, A. De Benedetti, R. Cester, A. De Marco Trabucco, M. I. Ferrero, A. Marzari-Chiesa, B. Quassiati, G. Rinaudo, M. Vigone, and A. E. Werbrouck, Study of Three-Body Leptonic K^+ Decay Modes, Presented at the Sienna Conference, September 1963 (to be published in the Proceedings).

18. D. Cutts, T. Elioff, and R. Stiening, Phys. Rev. 138, B 969 (1965).

19. G. Gidal, W. M. Powell, R. March, and S. Natali, Phys. Rev. Letters 13, 95 (1964);
G. Gidal, R. March, and S. Natali, Bull. Am. Phys. Soc. 9, 80 (1964).

20. V. A. Smirnitski and A. O. Weissenberg, Phys. Rev. Letters 12, 233 (1964).

21. F. S. Shaklee, G. L. Jensen, B. P. Roe, and D. Sinclair, Phys. Rev. 136, B 1423 (1964);
F. S. Shaklee, G. L. Jensen, B. P. Roe, and D. Sinclair, Bull. Am. Phys. Soc. 9, 34 (1964);
F. S. Shaklee, The Branching Ratios of the Positive K Meson (Ph.D. Thesis), University of Michigan, ORA Project 04938, March 1964 (unpublished).

22. A. C. Callahan, U. Camerini, R. L. Hantman, R. H. March, D. Murphree, G. Gidal, G. E. Kalmus, W. M. Powell, R. T. Pu, C. L. Sandler, S. Natali, and M. Villani, Measurement of $K\mu_3^+$ Decay Parameters (to be submitted to Phys. Rev.).

23. A. H. Rosenfeld, A. Barbaro-Galtieri, W. H. Barkas, P. L. Bastien, J. Kirz, and M. Roos, Rev. Mod. Phys. 36, 977 (1964);
also updated as Lawrence Radiation Laboratory Report UCRL-8030, Part I, March 1965 (unpublished);
see also W. H. Barkas, A. H. Rosenfeld, P. L. Bastien, and J. Kirz, Lawrence Radiation Laboratory Report UCRL-8030 Rev., April 1963 (unpublished).

24. J. H. Christenson, J. W. Cronin, V. L. Fitch, and R. Turlay, Phys. Rev. Letters 13, 138 (1964);
also see A. Abashian, R. J. Abrams, D. W. Carpenter, G. P. Fisher, B. M. K. Nefkens, and J. H. Smith, Phys. Rev. Letters 13, 243 (1964);
W. Galbraith, G. Manning, A. E. Taylor, B. D. Jones, J. Malos, A. Astbury, N. H. Lipman, and T. G. Walker, Phys. Rev. Letters 14, 383 (1965);
X. De Bouard, D. Dekkers, B. Jordan, R. Mermod, T. R. Willits, K. Winter, P. Scharff, L. Valentin, M. Vivorgent, and M. Bott-Bodenhausen, Phys. Letters 15, 58 (1965).

25. F. Zacharaisen and G. Zweig, Phys. Rev. Letters 14, 794 (1965).

26. S. L. Glashow, Phys. Rev. Letters 14, 35 (1965).

27. L. Wolfenstein, Phys. Rev. Letters 13, 562 (1964).

28. J. Bernstein, N. Cabibbo, and T. D. Lee, Phys. Letters 12, 146 (1964).

29. R. G. Sachs, Phys. Rev. Letters 13, 286 (1964).

30. N. Cabibbo, Phys. Letters 12, 137 (1964).

31. N. Cabibbo, Phys. Rev. Letters 14, 965 (1965).

32. U. Camerini, R. L. Hantman, R. H. March, D. Murphree, G. Gidal, G. E. Kalmus, W. M. Powell, R. T. Pu, C. L. Sandler, S. Natali, and M. Villani, Phys. Rev. Letters 14, 989 (1965).

33. G. E. Kalmus, G. Gidal, W. M. Powell, C. L. Sandler, U. Camerini, R. March, D. Murphree, and S. Natali, Bull. Am. Phys. Soc. 10, 91 (1965).

34. V. Bisi, G. Borreani, A. Marzari-Chiesa, G. Rinaudo, M. Vigone, and A. E. Werbrouck, $K_{\mu 3}$ Branching Ratio and μ^+ Energy Spectrum, Istituto di Fisica Università-Torino preprint, March 1965 (submitted to Physical Review).

35. G. L. Jensen, C. T. Murphy, and B. P. Roe, Phys. Rev. 138, B 1507 (1965).

36. G. E. Kalmus, A. Kernan, U. Camerini, and C. Henderson, Analysis of the Decay $K^+ \rightarrow \pi^0 + e^+ + \nu$, Lawrence Radiation Laboratory Report UCRL-11553, July 1964 (to be published in Proceedings of the International Conference on High-Energy Physics, Dubna, 1964).

37. J. L. Brown, J. A. Kadyk, G. H. Trilling, R. T. Van de Walle, B. P. Roe, and D. Sinclair, Phys. Rev. Letters 7, 423 (1961); see also Experimental Study of the K^+_{e3} Decay Interaction, Lawrence Radiation Laboratory Report UCRL-9892, Oct. 1961 (unpublished).

38. D. Luers, I. S. Mittra, W. J. Willis, and S. S. Yamamoto, Phys. Rev. 133, B1276 (1964); D. Luers, I. S. Mittra, W. J. Willis, and S. S. Yamamoto, Phys. Rev. Letters 7, 255 (1961).

39. P. Dennery and H. Primakoff, Phys. Rev. 131, 1334 (1963).

40. R. P. Feynman and M. Gell-Mann, Phys. Rev. 109, 193 (1958).

41. E. C. G. Sudarshan and R. E. Marshak in Proceedings of the Padua-Venice Conference on Mesons and Newly Discovered Particles, September 1957, (Societa Italiana di Fisica, Padua-Venice, 1958); Phys. Rev. 109, 1860 (1958).

42. W. M. Powell, W. B. Fowler, and L. O. Oswald, Rev. Sci. Instr. 29, 874 (1958).

43. W. M. Powell, L. O. Oswald, G. Griffin, and F. Swartz, Rev. Sci. Instr. 34, 1426 (1963).

44. G. Goldhaber, S. Goldhaber, J. Kadyk, T. F. Stubbs, D. Stork, and H. Ticho, Separated K^+ Beams, Lawrence Radiation Laboratory Report Bev-483, Feb. 1960 (unpublished).

45. We used Professor George Trilling's program for the range-energy relations. They were calculated by using the Bethe-Bloch formula.

46. Verification of this number comes from Professor Robert March and co-workers at the University of Wisconsin. They have studied the ionization of K^+ mesons in our film by looking at K^+_τ decays. First, they decided without looking at the outgoing prongs whether the K^+ had decayed at rest, and then checked whether the decay had occurred at rest by examining the momentum balance of the outgoing prongs.

47. A separate scan was done for the $K^+_{\mu 3}$ (2γ ray) events, and the events were analyzed as part of another experiment (see reference 22).

48. Andrew Callahan and Robert March, (University of Wisconsin, private communication) report seeing in a sample of 320 $K_{\pi 2}$ decays seven possible candidates with short ranges for a $K_{\pi 2}$. The events were from the same bubble chamber film as that in the experiment reported in this paper. Also, Ronald Hantman and Robert March have made an evaluation of the fraction of $\pi\mu e$ decay chains not seen on the end of π^+ mesons from K^+_τ decays. They obtain results compatible with our measurement of $F_{\substack{no \\ \pi\mu e}} = (13 \pm 3)\%$;
Walter H. Barkas, (Lawrence Radiation Laboratory, private communication) reports seeing no evidence for elastic small-angle scatterings of π^+ from a sample of 50 $K_{\pi 2}$ decays stopping in nuclear emulsion.

49. H. S. White, Data Processing for Bubble Chambers, Lawrence Radiation Laboratory Report UCRL-9475, Nov. 1960 (unpublished);
also see Reference Manual for FOG-CLOUDY-FAIR Bubble Chamber Data Processing System, Lawrence Radiation Laboratory Document UCID-1340 (unpublished).

50. R. S. Burington and D. C. May, Handbook of Probability and Statistics with Tables (Handbook Publishers, Inc. Sandusky, Ohio, 1953), p. 176.

51. G. E. Kalmus, A. Kernan, R. T. Pu, W. M. Powell, and R. Dowd, Phys. Rev. Letters 13, 99 (1964).

52. Anne Kernan (Lawrence Radiation Laboratory, private communication) studied, in reference 51, the total π^+ inelastic cross section in C_3F_8 up to $E_{\pi\ MAX} = 188$ MeV, by measuring the outgoing π^+ prongs in approximately 600 K^+_τ decays, in order to determine the background correction for the π^+ spectrum in $K^+_{\tau'}$ decay.

53. N. Cabibbo, Nuovo Cimento 11, 837 (1959).

54. N. Cabibbo (Lawrence Radiation Laboratory) private communication.

55. S. Taylor, G. Harris, J. Orear, J. Lee, and P. Baumel, Phys. Rev. 114, 359 (1959).

56. T. H. Groves, P. R. Klein, and V. Vanderburg, Phys. Rev. 135, B 1269 (1964).

APPENDICES

A. Some Algebraic Expressions

We display explicitly the form of A, B and C in (2.8). Using (2.3) and (2.5) along with the definition $\xi = f_-/f_+$, we can write

$$\frac{(d\Gamma\,(E_\mu)/dE_\mu)}{C'\,f_+^2} = (E_\mu^2 - m_\mu^2)^{1/2}\,\frac{(\Delta - m_\pi^2 - 2M_K E_\mu)^2}{(\Delta - 2M_K E_\mu)}\left\{M_K E_\mu + (1+\xi^2)\times\right.$$

$$\left.\times\left[\frac{1}{4}\,m_\mu^2\,\frac{M_K E_\mu - m_\mu^2}{\Delta - 2M_K E_\mu}\right] + \xi\left[\frac{1}{2}\,m_\mu^2\left(\frac{2M_K^2 + m_\mu^2 - 3\,M_K\,E_\mu}{\Delta - 2M_K E_\mu}\right)\right]\right\}.$$

Let

$$a_o = (E_\mu^2 - m_\mu^2)^{1/2},$$

$$a_1 = \frac{(\Delta - m_\pi^2 - 2M_K E_\mu)^2}{(\Delta - 2M_K E_\mu)},$$

$$a_2 = \frac{1}{4}\,m_\mu^2\left(\frac{M_K E_\mu - m_\mu^2}{\Delta - 2M_K E_\mu}\right),$$

$$a_3 = \frac{1}{2}\,m_\mu^2\left(\frac{2M_K^2 + m_\mu^2 - 3M_K E_\mu}{\Delta - 2M_K E_\mu}\right),$$

$$a_4 = a_o\,a_1.$$

Then

$$\frac{(d\Gamma\,(E_\mu)/dE_\mu)}{C'\,f_+^2} = (a_4\,M_K\,E_\mu + a_4\,a_2) + (a_4\,a_3)\xi + (a_4\,a_2)\xi^2$$

$$= A(E_\mu) + B(E_\mu)\xi + C(E_\mu)\xi^2.$$

B. Range-Momentum Tables for C_3F_8

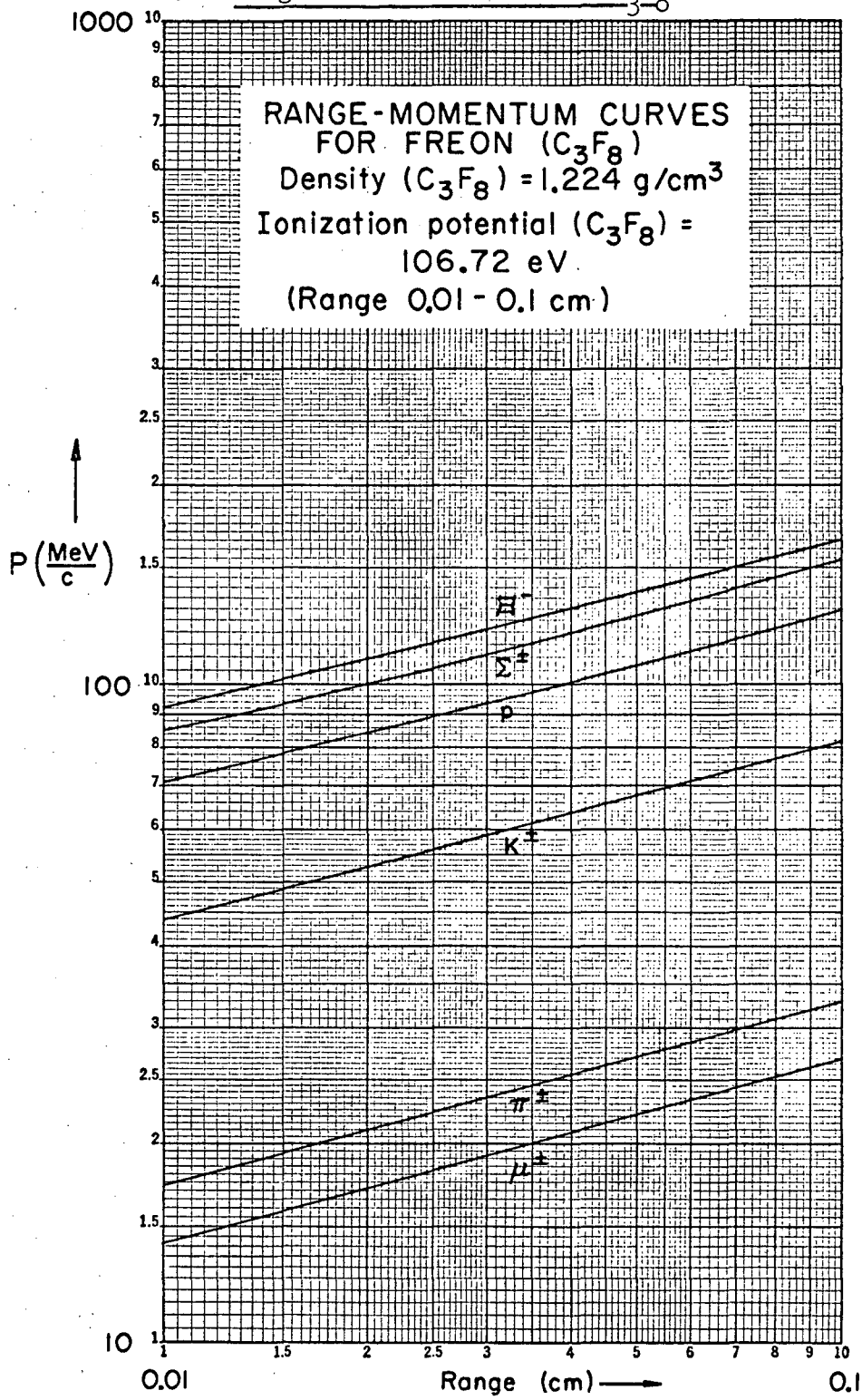

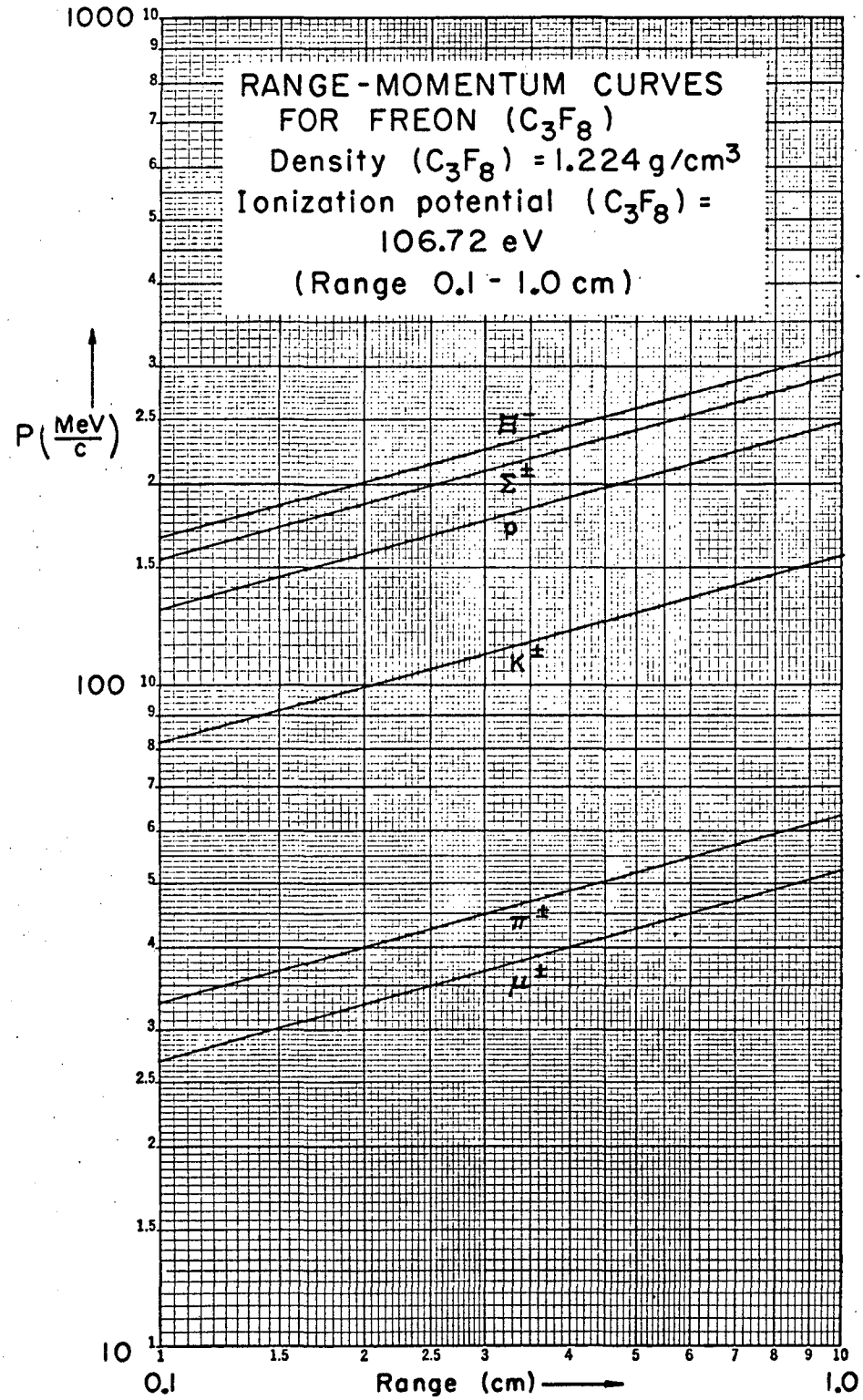
RANGE-MOMENTUM CURVES
FOR FREON (C_3F_8)
Density (C_3F_8) = 1.224 g/cm^3
Ionization potential (C_3F_8) =
106.72 eV
(Range 0.1 - 1.0 cm)
P (MeV/c)
1000
100
10
Ξ^-
$\Sigma^\pm$
p
$K^\pm$
$\pi^\pm$
$\mu^\pm$
0.1
Range (cm)
1.0

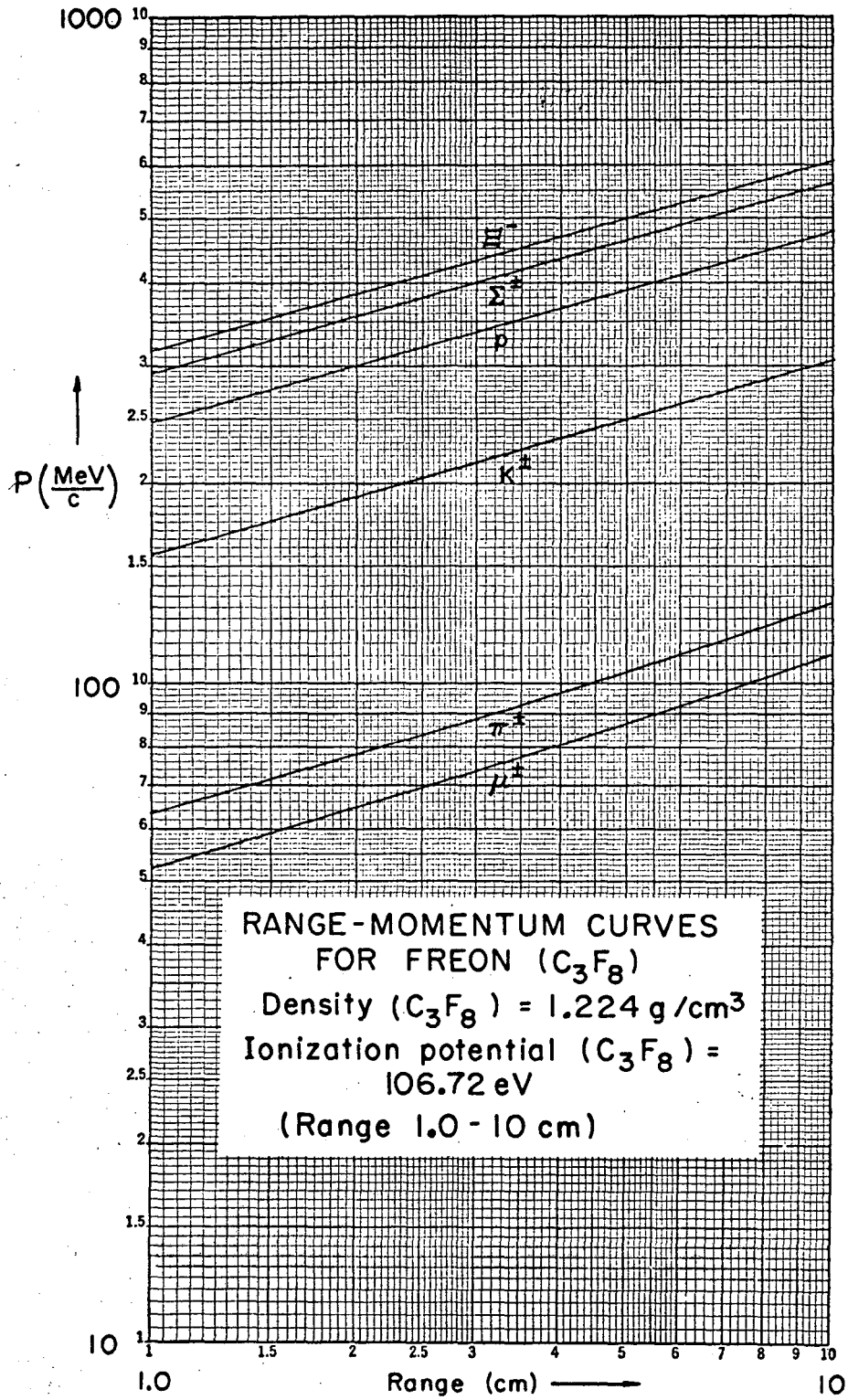
1000
100
10
1.0
10
P (MeV/c)
Range (cm)
Ξ⁻
Σ±
p
K±
π±
μ±
RANGE-MOMENTUM CURVES
FOR FREON (C3F8)
Density (C3F8) = 1.224 g/cm3
Ionization potential (C3F8) =
106.72 eV
(Range 1.0 - 10 cm)

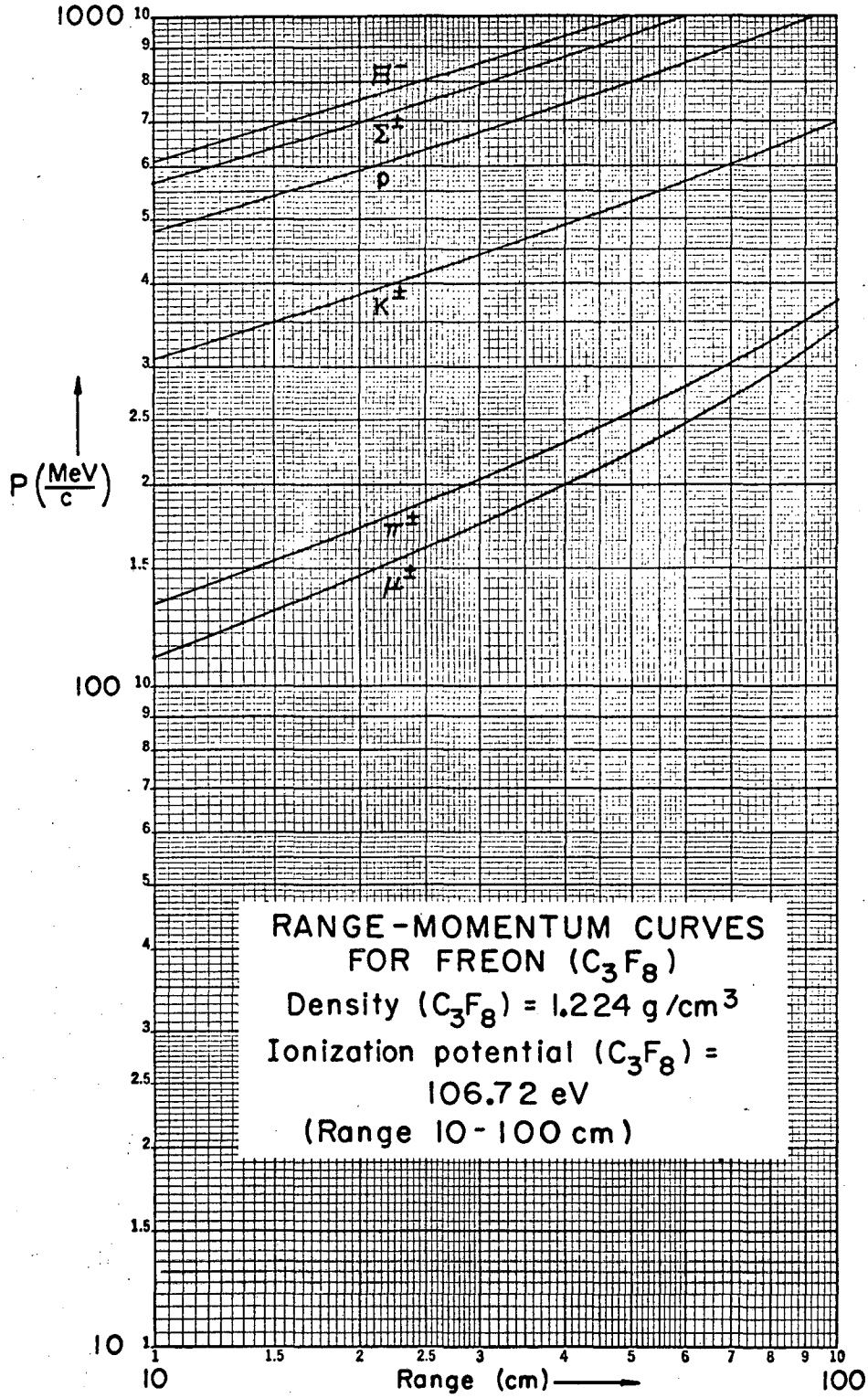
1000
100
10
P (MeV/c)
Ξ⁻
Σ±
p
K±
π±
μ±
RANGE-MOMENTUM CURVES
FOR FREON (C_3F_8)
Density (C_3F_8) = 1.224 g/cm³
Ionization potential (C_3F_8) =
106.72 eV
(Range 10-100 cm)
10
Range (cm)
100

C. LIST OF TABLES AND FIGURE CAPTIONS

TABLE I. Summary of Experimental Papers.

TABLE II. K^+ Decay Modes and Kinematical Data.
Ranges have been calculated; the other data is taken from Reference 23.

TABLE III. Experimental Data and Background.
(High energy part of μ^+ spectrum, $106 \leq T_\mu \leq 134$ MeV).

TABLE IV. Experimental Data and Background.
(Low and intermediate energy portion of μ^+ spectrum $23 \leq T_\mu \leq 94$ MeV).

TABLE V. General Form of Analysis Functions.

Fig. 1. Feynman diagram for $K\mu_3^+$ decay.

Fig. 2. Theoretical μ^+ kinetic energy spectrum for $K\mu_3^+$ decay. The various curves are parameterized by ξ the form factor ratio, and each is normalized to a total area of unity.

Fig. 3. A representative photograph of stopping K^+ decays. This photograph shows $K_{L_3}^+$ decays, $K\mu_2^+$ decay, and $K\pi_2^+$ decay with π^+ interacting in flight.

Fig. 4. A typical photograph of K^+ mesons stopping in the Berkeley 30-inch heavy-liquid bubble chamber. This picture shows the $K\mu_3^+$ decay, $K\pi_2^+$ and K_τ^+ decays, and also illustrates the μe and the $\pi\mu e$ decay chains.

Fig. 5. Experimental beam arrangement. The symbols T, C, BM, SP, Q, and S refer respectively to the proton target, the collimator, bending magnet, spectrometer, quadrupole magnet, and slit.

Fig. 6. Vertical lens and focussing diagram. The symbols T, C, BM, SP, Q, and S refer respectively to the proton target, the collimator, bending magnet, spectrometer, quadrupole magnet, and slit. The positions of the P, K, and π are not to scale.

Fig. 7. Typical π-K separation curve at the second slit. The abscissa is in units of shunt voltage for the magnet of the second spectrometer.

Fig. 8. Sketch of a K^+_τ, decay.

Fig. 9. The solid lines are a histogram of experimentally observed $K\mu^+_3$ events plotted as a function of R_μ, the range of the muon. In each interval the area above the dotted lines represents the background corrections, while the area below the dotted lines represents the number of $K\mu^+_3$ events. The percentage contribution of each type of background is indicated over its region of importance.

Fig. 10. Histogram of π^+ kinetic energy from 10 to 53 MeV in $K^+ \rightarrow \pi^+ + \pi^0 + \pi^0$. The smooth curves are the distributions expected for a constant decay amplitude having a linear dependence on T_{π^+}. The curves are normalized to the region from 10 to 53 MeV.

Fig. 11. Fraction of $K\mu^+_2$ (K^+ flt.) events as a function of the μ^+ length. The curves depend on the residual range of the K^+, that is, the length of the K^+ track in C_3F_8 from its decay origin to the place it would have stopped, if it had not decayed in flight.

Fig. 12. Fraction of $K^+_{\pi 2}$ (π^+ flt.) events as a function of $\theta_{\pi\mu}$ (the angle between the π^+ and the μ^+) and $L_{(\pi + \mu)}$ (the combined length of the π and the μ).

Fig. 13. The ratio of the $K^+_{\mu\gamma}$ to the $K^+_{\mu 2}$ decay rate as a function of the kinetic energy of the muon.

Fig. 14. The potential path length correction as a function of the length of the μ^+. The curve gives the probability for the μ^+ track to stop anywhere in the available 4π solid angle within the chamber's fiducial volume.

Fig. 15. The potential path length correction factors used in analysis. The μ^+ detection efficiency curves start at $F_{PPL_\mu} = 0.6$, because the Monte Carlo tracks generated were restricted to lie within ± 37° of the horizontal plane. This meant that only 60% of the total 4π solid angle was available for the decays.

Fig. 16. Plot of χ^2 as a function of ξ. The parameter ξ is used to fit the μ^+ kinetic energy spectrum over the interval $8 \leq L_\mu \leq 28$ cm, $41 \leq T_\mu \leq 94$ MeV.

Fig. 17. A plot of the $K^+_{\mu 3}$ branching ratio as a function of the parameter ξ. The curves labeled "$BR_{K_{\mu 3}}$ Experimental Values" were generated by simultaneously fitting the experimental μ^+ spectral shape and the area under the spectral curve. The other set of curves are theoretical curves which are based on the assumption of μe-universality and require experimental information on the K^+_{e3} branching ratio.

Fig. 18. The μ^+ spectrum has been fitted by a two parameter maximum likelihood function. This plot shows the projection of the likelihood function $L(\xi_{RE}, \xi_{IM})$ onto the complex ξ-plane.

Fig. 19. A plot showing the relationship between ξ_{RE} and ξ_{IM} as a function of the experimentally determined ratio $R = BR_{K\mu_3}/BR_{Ke_3}$.

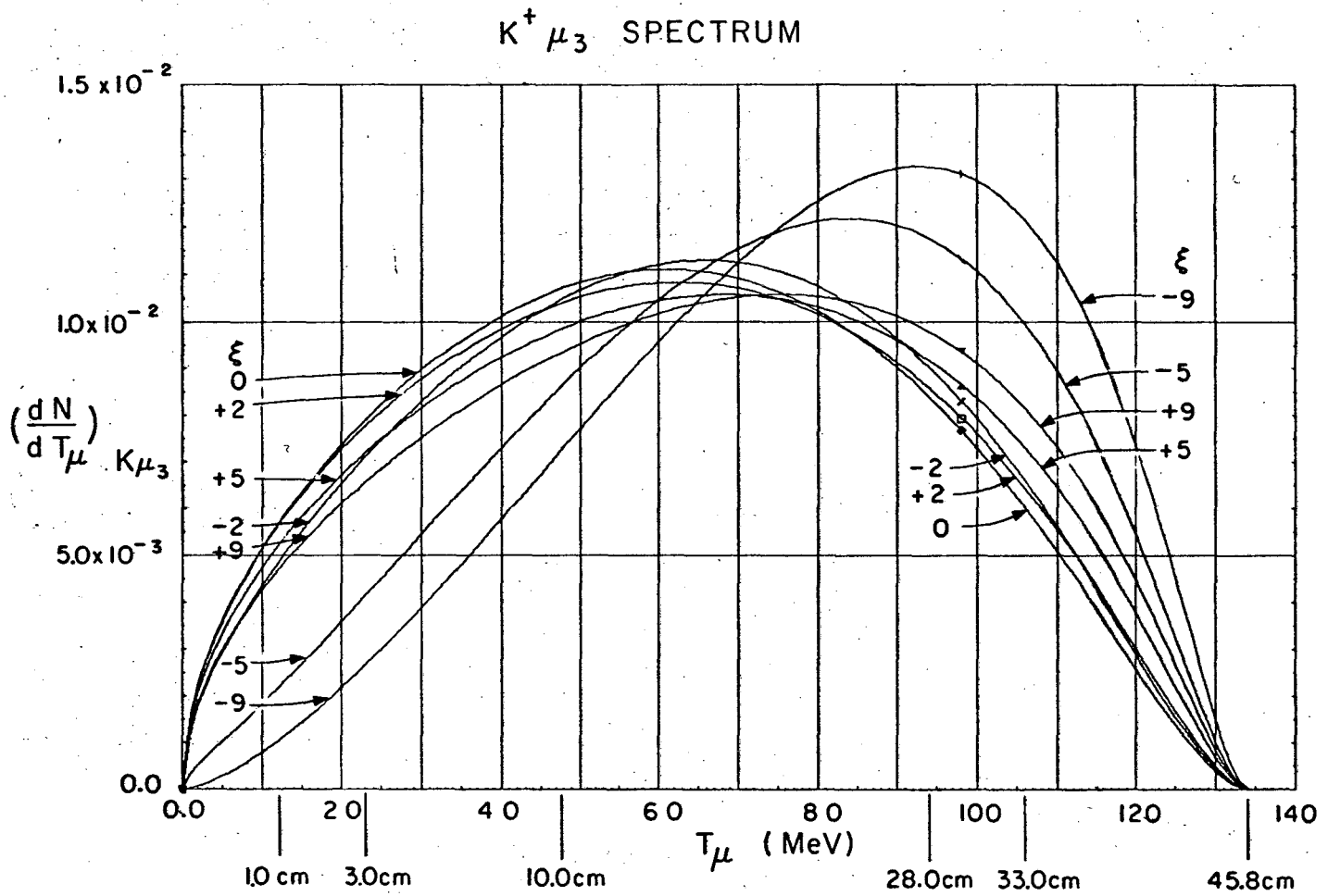

Fig. 2. Theoretical μ^+ kinetic energy spectrum for $K^+_{\mu 3}$ decay. The various curves are parameterized by ξ, the form factor ratio, and each is normalized to a total area of unity.

MU-35050

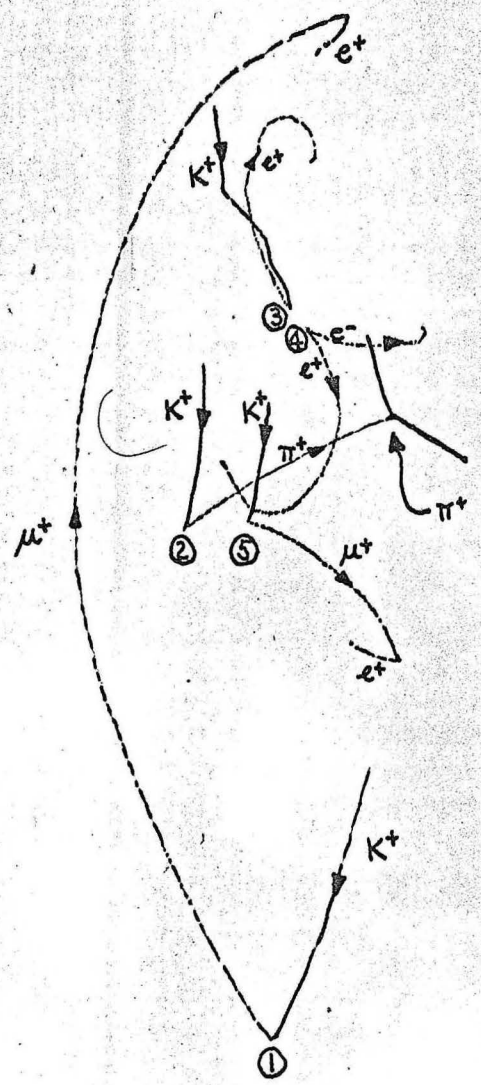

① $K^+ \rightarrow \mu^+ + \nu$ ($K^+_{\mu 2}$ Decay), $L_\mu = 54.3$ cm

② $K^+ \rightarrow \pi^+ + \pi^0$ ($K^+_{\pi 2}$ Decay) with π^+ interaction in flight

③ $K^+ \rightarrow \pi^0 + e^+ + \nu$ (K^+_{e3} Decay) with 1γ from π^0 converting

and ④ $\pi^0 \rightarrow \gamma + \gamma$, γ + nucleus $\rightarrow$ $\underbrace{e^+ + e^-}_{\gamma \text{ pair}}$ + $\underbrace{\text{nucleus}}_{\text{not visible}}$

⑤ $K^+ \rightarrow \pi^0 + \mu^+ + \nu$ ($K^+_{\mu 3}$ Decay), here $L_\mu = 10.5$ cm

ZN-5297

Fig. 3. A representative photograph of stopping K^+ decays. This photograph shows $K^+_{L_3}$ decays, $K^+_{\mu_2}$ decay, and $K^+_{\pi_2}$ decay with π^+ interacting in flight.

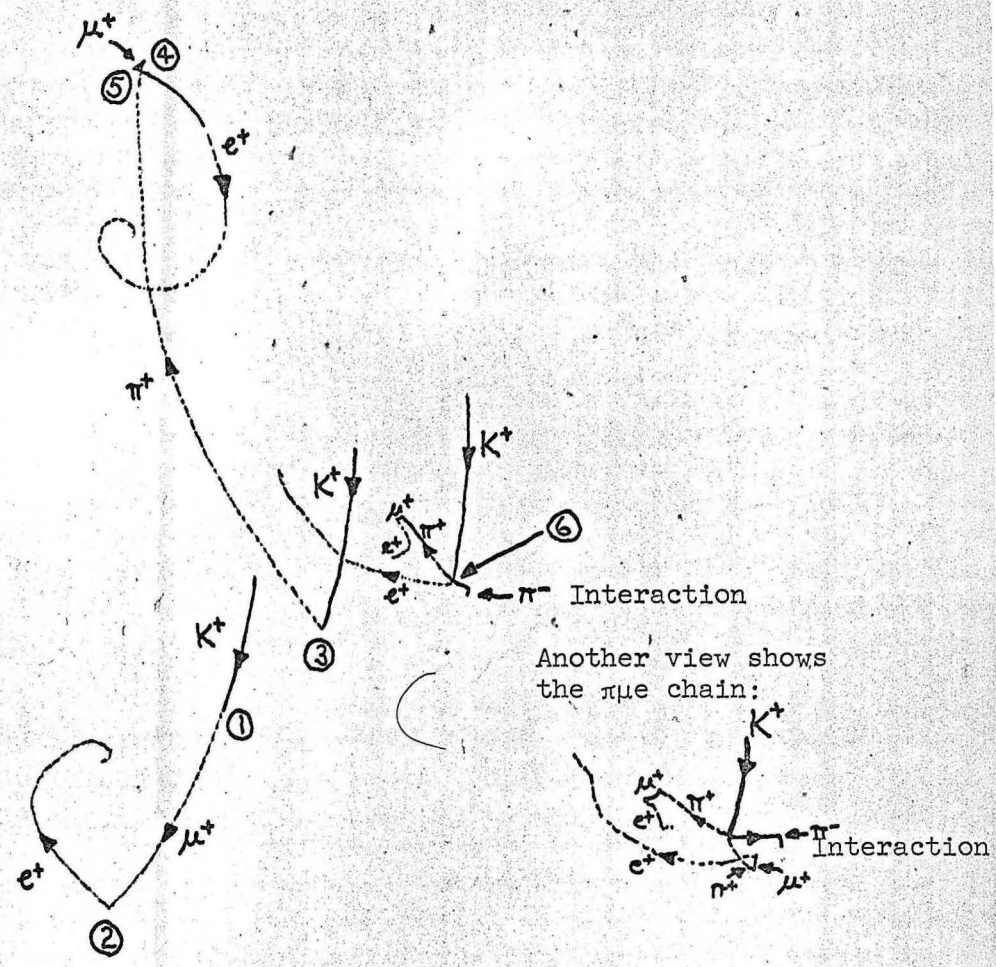

(1) $K^+ \rightarrow \pi^o + \mu^+ + \nu$ ($K^+_{\mu 3}$ Decay)
and (2) $\mu^+ \rightarrow e^+ + \nu + \bar{\nu}$ (μe Decay) } Here $L_\mu = 12.2$ cm

(3) $K^+ \rightarrow \pi^+ + \pi^o$ ($K^+_{\pi 2}$ Decay), $L_{\pi^+} = 30.5$ cm

and (4) $\pi^+ \rightarrow \mu^+ + \nu$ ($\pi\mu$ Decay)
and (5) $\mu^+ \rightarrow e^+ + \nu + \bar{\nu}$ (μe Decay) } Notice "$\pi\mu e$ chain" $L_\mu = 1.44$ mm

(6) $K^+ \rightarrow \pi^+ + \pi^+ + \pi^-$ (K^+_τ Decay), in this view one of the $\pi\mu e$ chains is not visible.

ZN-5296

Fig. 4. A typical photograph of K^+ mesons stopping in the Berkeley 30-inch heavy-liquid bubble chamber. This picture shows the $K^+_{\mu 3}$ decay, $K^+_{\pi 2}$ and K^+_{τ} decays, and also illustrates the μe and the $\pi\mu e$ decay chains.

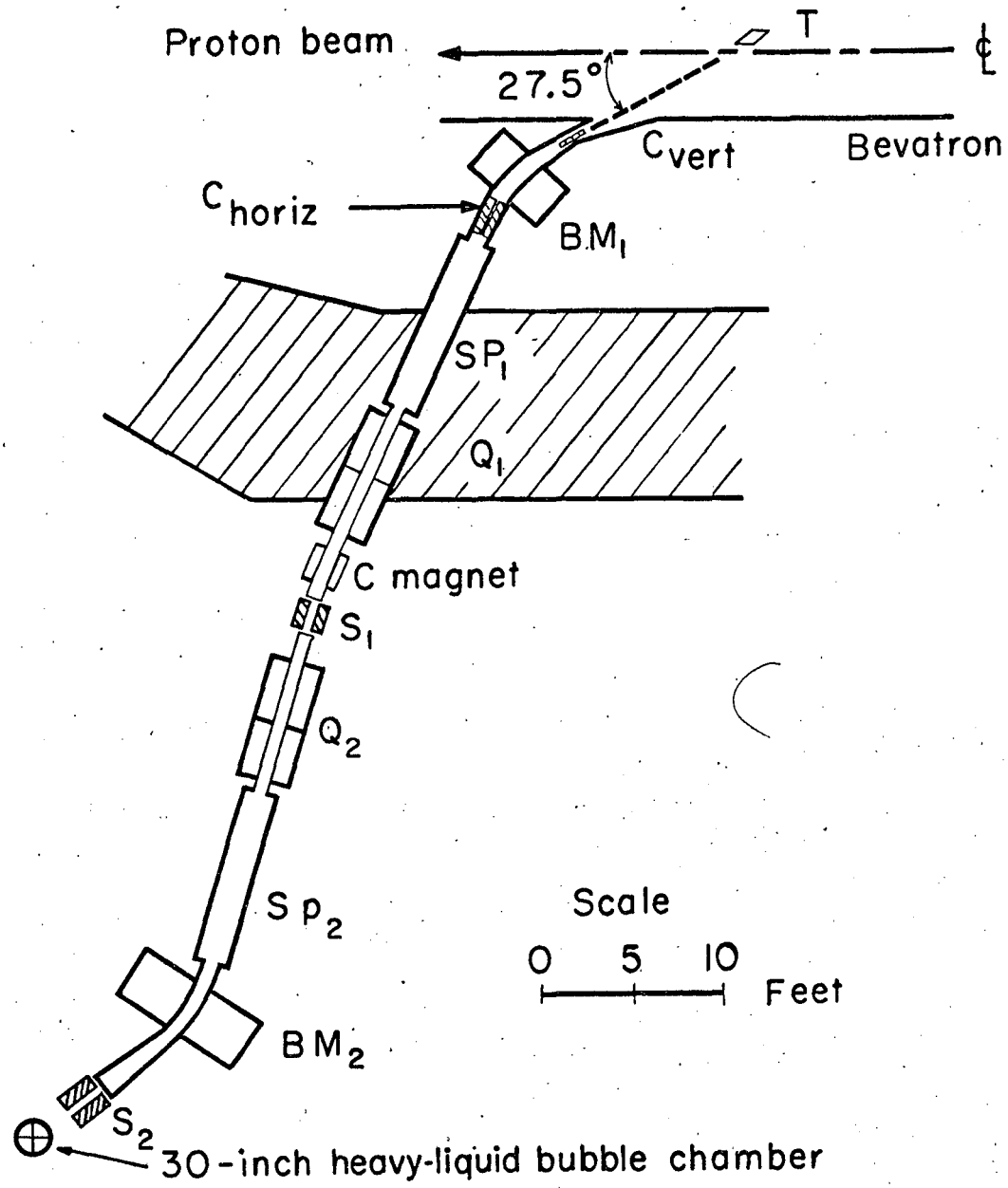

Fig. 5. Experimental beam arrangement. The symbols T, C, BM, SP, Q, and S refer respectively to the proton target, the collimator, bending magnet, spectrometer, quadrupole magnet, and slit.

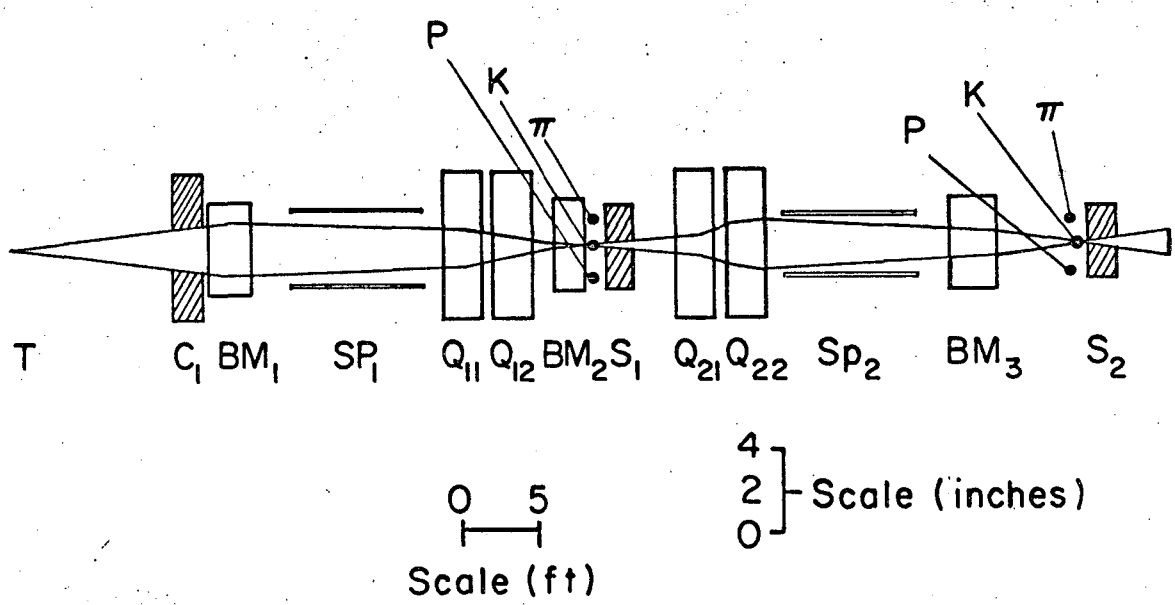

Fig. 6. Vertical lens and focussing diagram. The symbols T, C, BM, SP, Q, and S refer respectively to the proton target, the collimator, bending magnet, spectrometer, quadrupole magnet, and slit. The positions of the P, K, and π are not to scale.

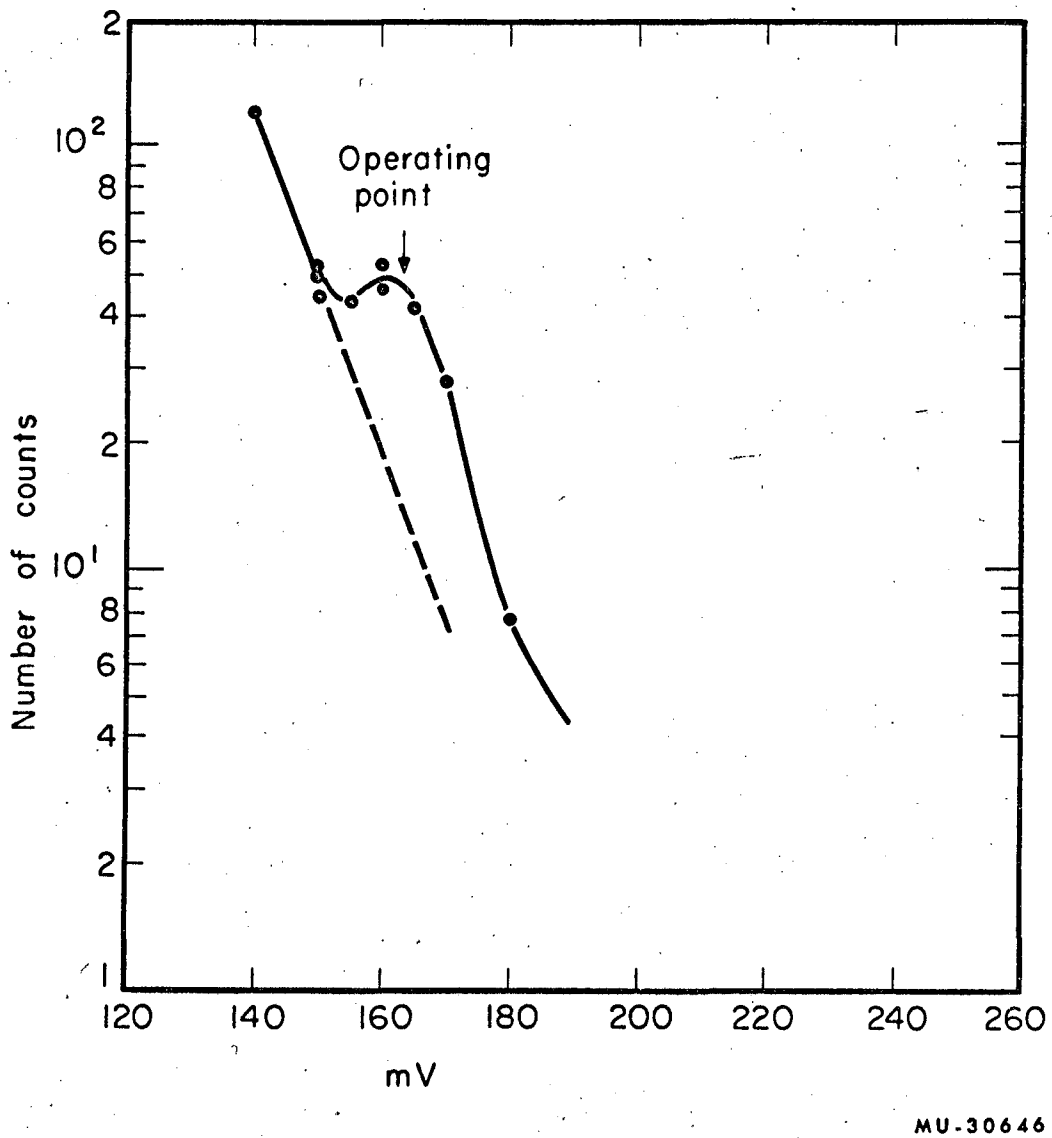

Fig. 7. Typical π-K separation curve at the second slit. The abscissa is in units of shunt voltage for the magnet of the second spectrometer.

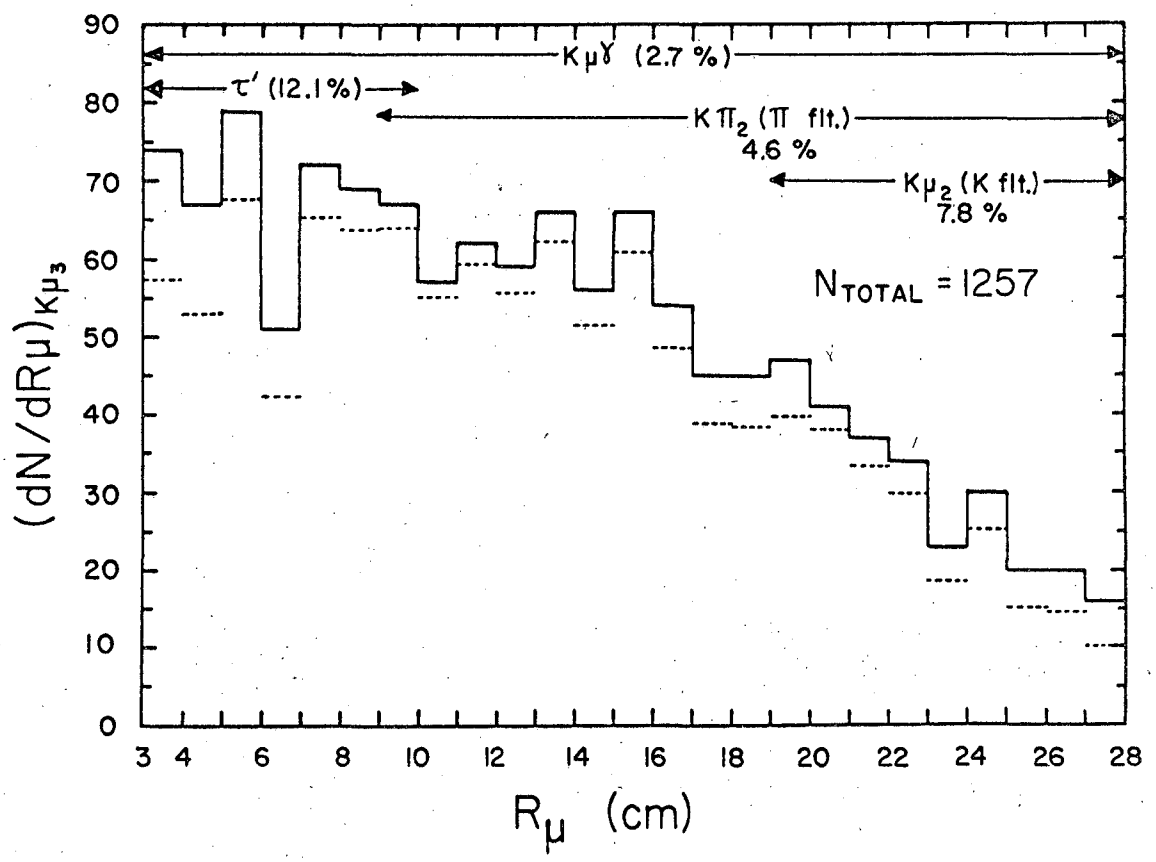

MU-36201

Fig. 9. The solid lines are a histogram of experimentally observed $K^+_{\mu 3}$ events plotted as a function of R_μ, the range of the muon. In each interval the area above the dotted lines represents the background corrections, while the area below the dotted lines represents the number of $K^+_{\mu 3}$ events. The percentage contribution of each type of background is indicated over its region of importance.

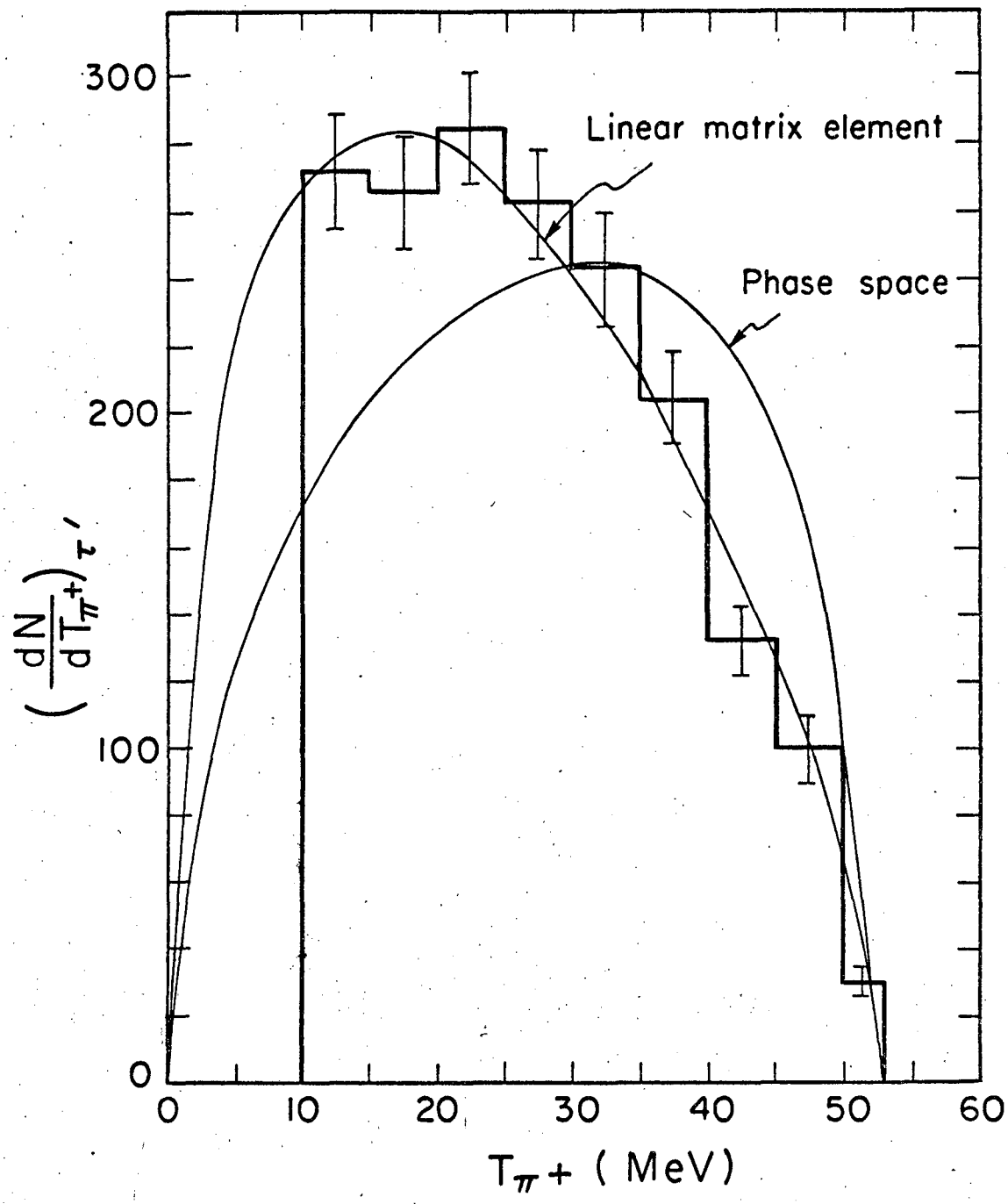

Fig. 10. Histogram of π^+ kinetic energy from 10 to 53 MeV in $K^+ \rightarrow \pi^+ + \pi^0 + \pi^0$. The smooth curves are the distributions expected for a constant decay amplitude having a linear dependence on T_{π^+}. The curves are normalized to the region from 10 to 53 MeV.

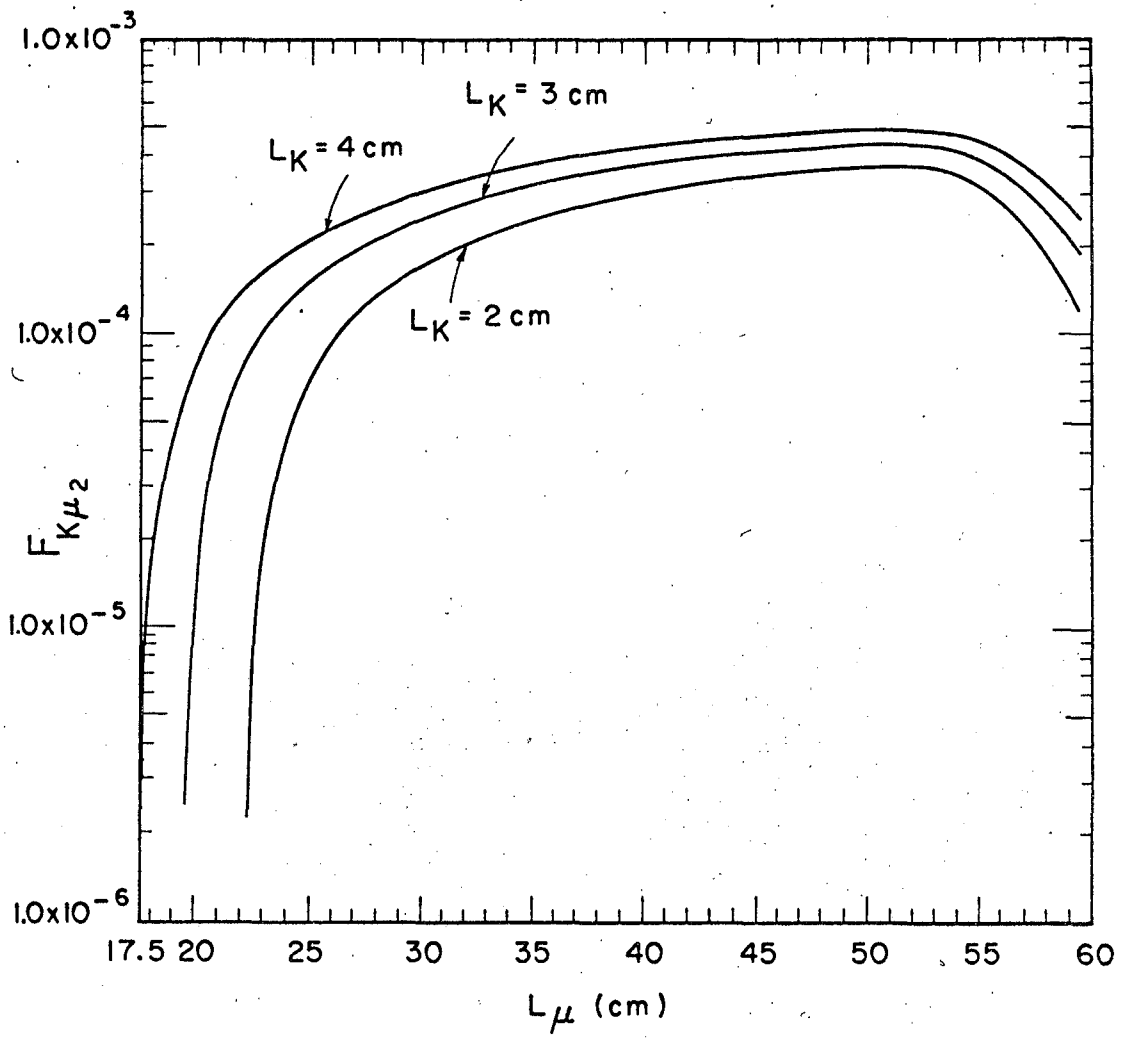

Fig. 11. Fraction of $K^+_{\mu 2}$ (K^+ flt.) events as a function of the μ^+ length. The curves depend on the residual range of the K^+, that is, the length of the K^+ track in C_3F_8 from its decay origin to the place it would have stopped, if it had not decayed in flight.

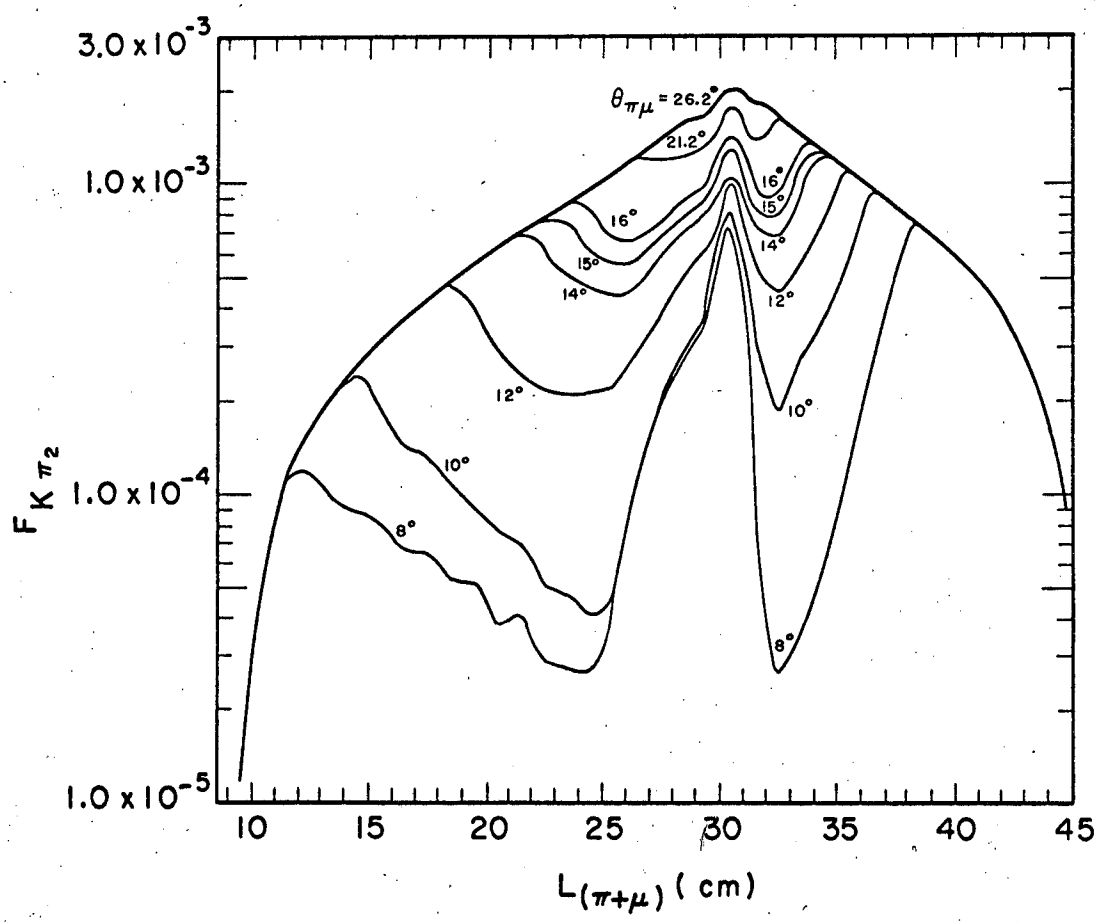

Fig. 12. Fraction of $K^+_{\pi 2}$ (π^+ flt.) events as a function of $\theta_{\pi\mu}$ (the angle between the π^+ and the μ^+) and $L_{(\pi + \mu)}$ (the combined length of the π and the μ).

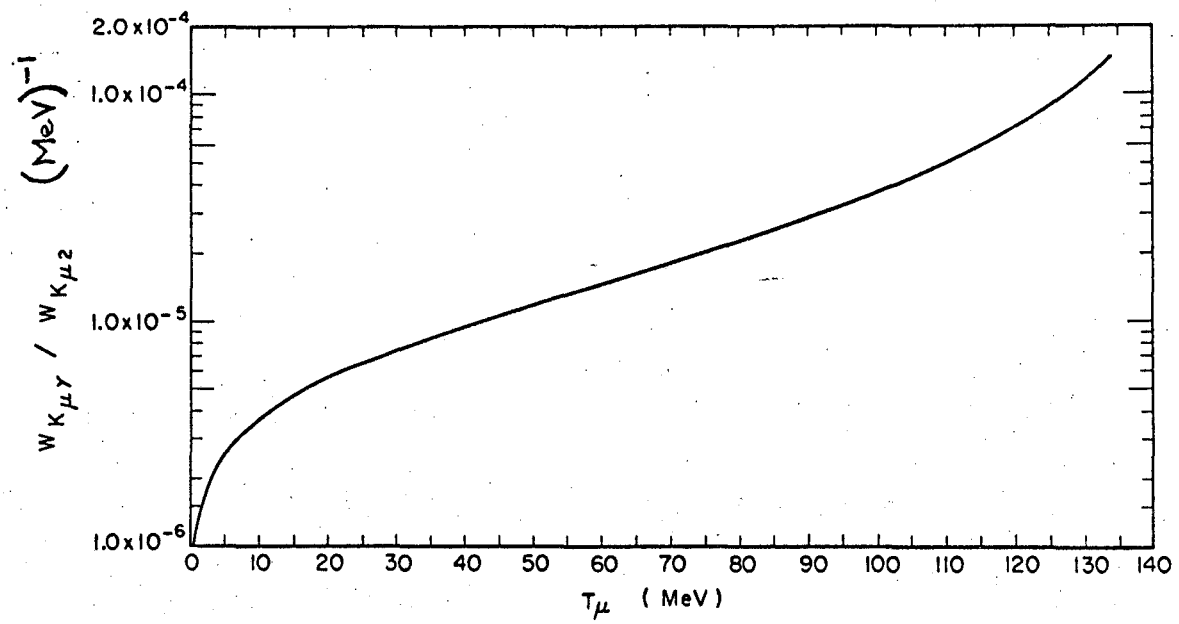

Fig. 13. The ratio of the $K^+_{\mu_\gamma}$ to the $K^+_{\mu_2}$ decay rate as a function of the kinetic energy of the muon.

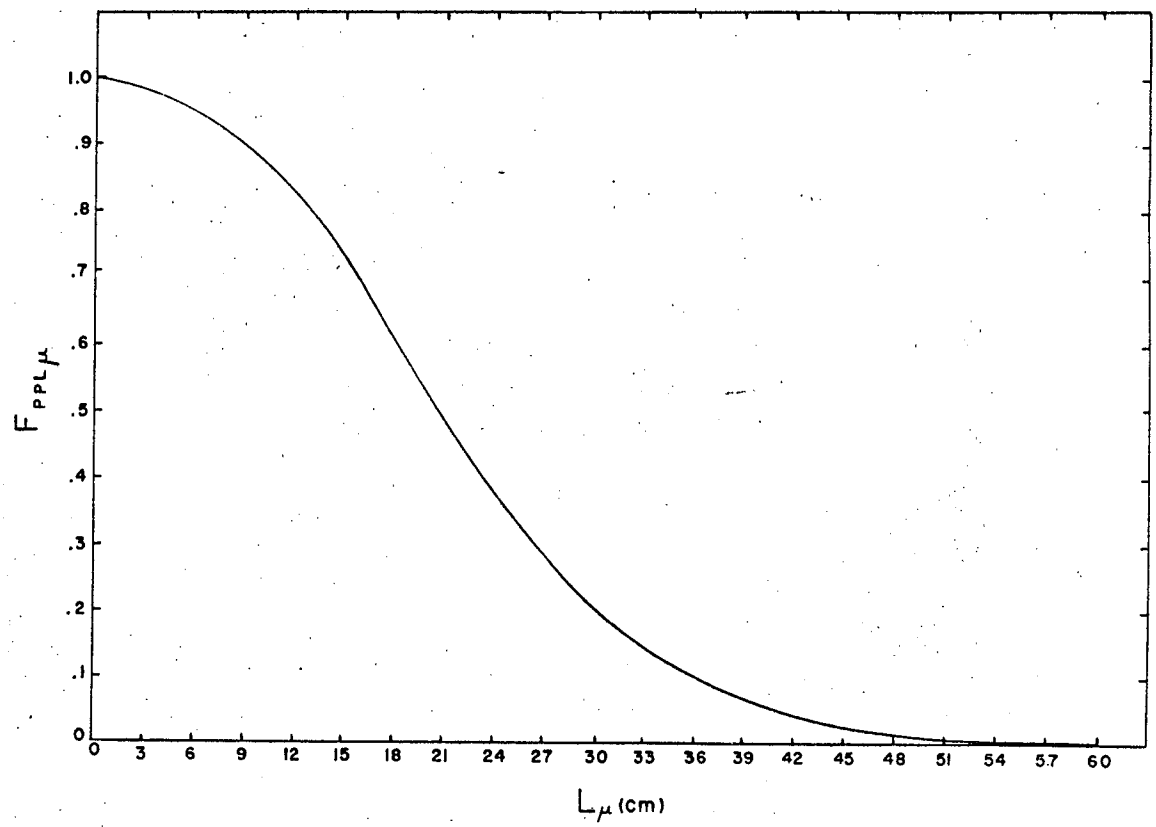

MU-36203

Fig. 14. The potential path length correction as a function of the length of the μ^+. The curve gives the probability for the μ^+ track to stop anywhere in the available 4π solid angle within the chamber's fiducial volume.

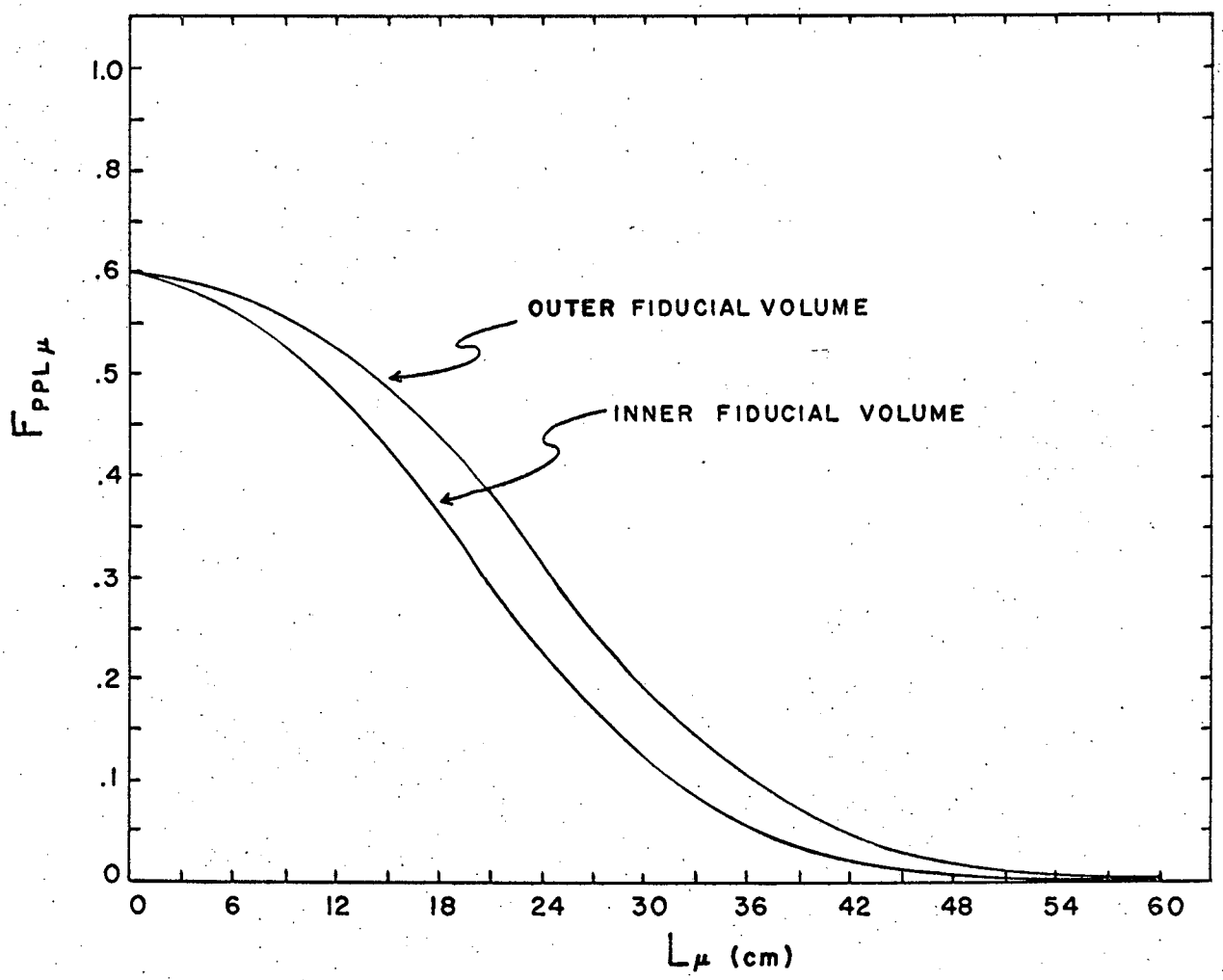

MUB-6821

Fig. 15. The potential path length correction factors used in analysis. The μ^+ detection efficiency curves start at $F_{PPL_\mu} = 0.6$, because the Monte Carlo tracks generated were restricted to lie within ± 37° of the horizontal plane. This meant that only 60% of the total 4π solid angle was available for the decays.

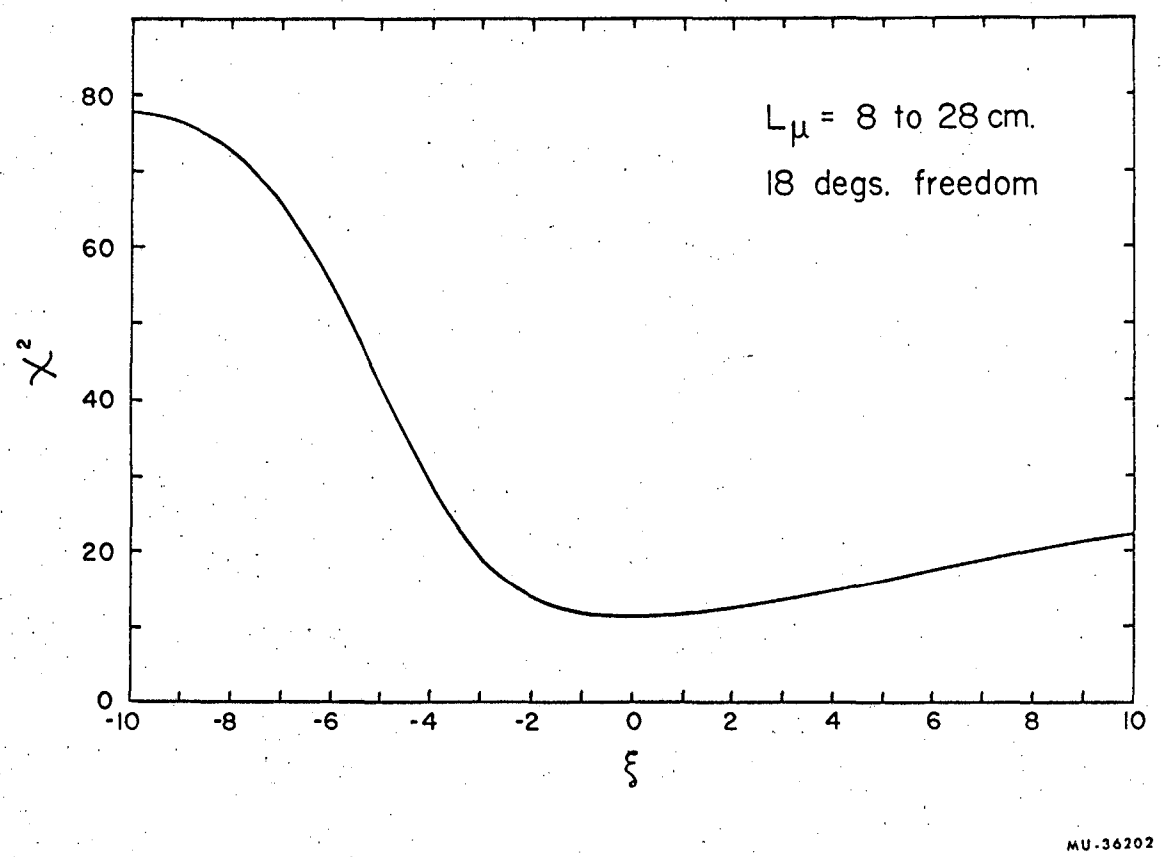

Fig. 16. Plot of χ^2 as a function of ξ. The parameter ξ is used to fit the μ^+ kinetic energy spectrum over the interval $8 \leq L_\mu \leq 28$ cm, $41 \leq T_\mu \leq 94$ MeV.

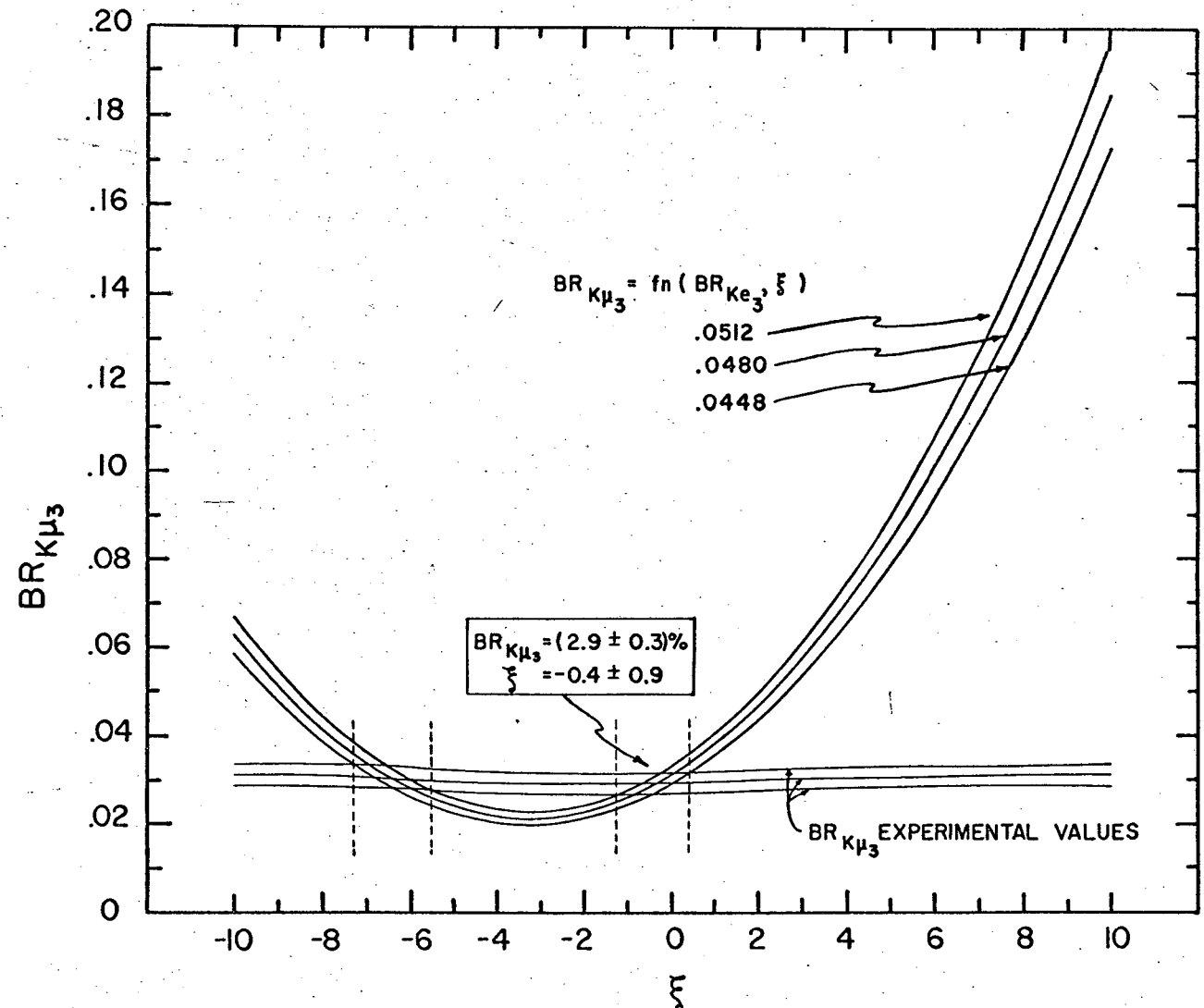

Fig. 17. A plot of the $K^+_{\mu 3}$ branching ratio as a function of the parameter ξ. The curves labeled "$BR_{K_{\mu 3}}$ Experimental Values", were generated by simultaneously fitting the experimental μ^+ spectral shape and the area under the spectral curve. The other set of curves are theoretical curves which are based on the assumption of μe-universality and require experimental information on the K^+_{e3} branching ratio.

MUB-6822

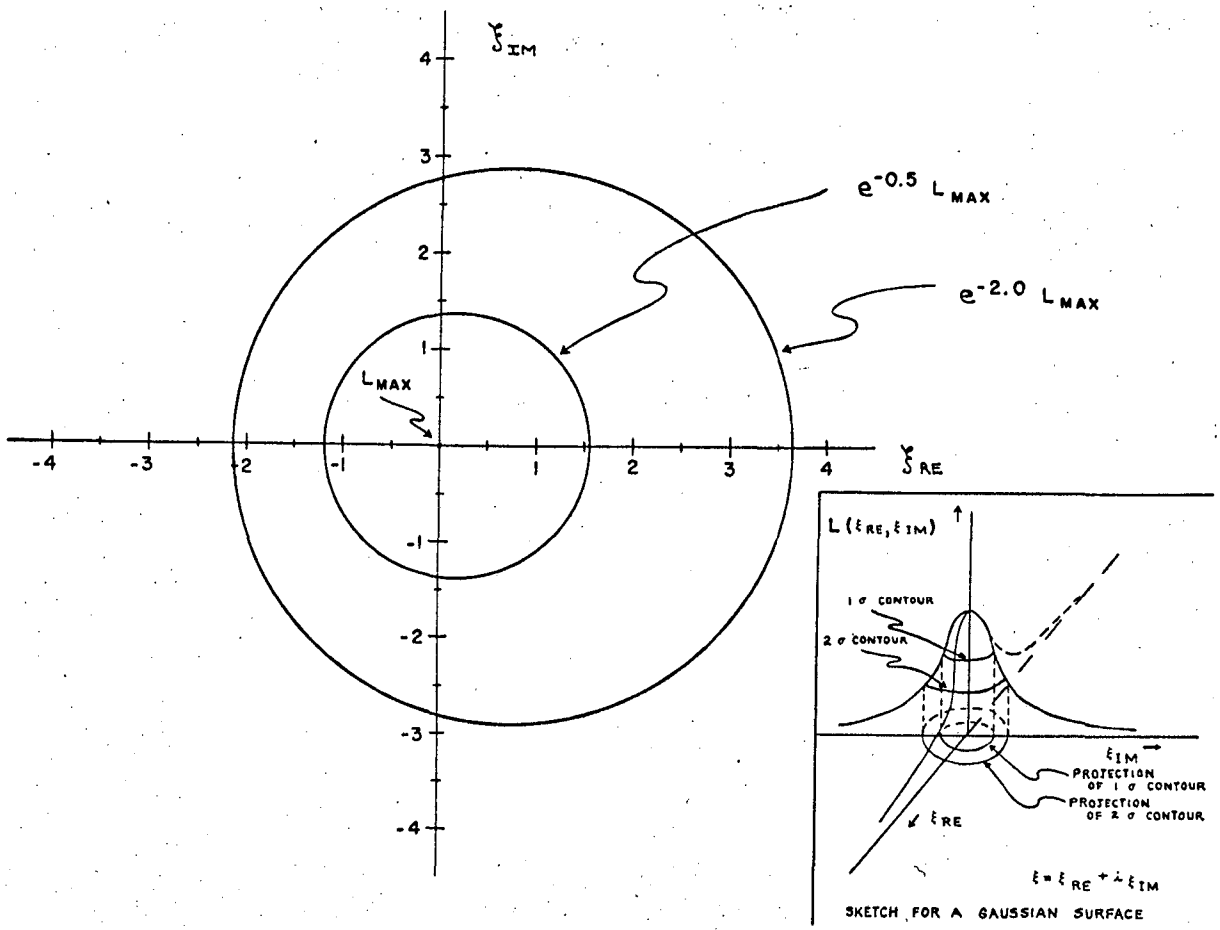

MUB-6820

Fig. 18. The μ^+ spectrum has been fitted by a two parameter maximum likelihood function. This plot shows the projection of the likelihood function $L(\xi_{RE}, \xi_{IM})$ onto the complex ξ-plane.

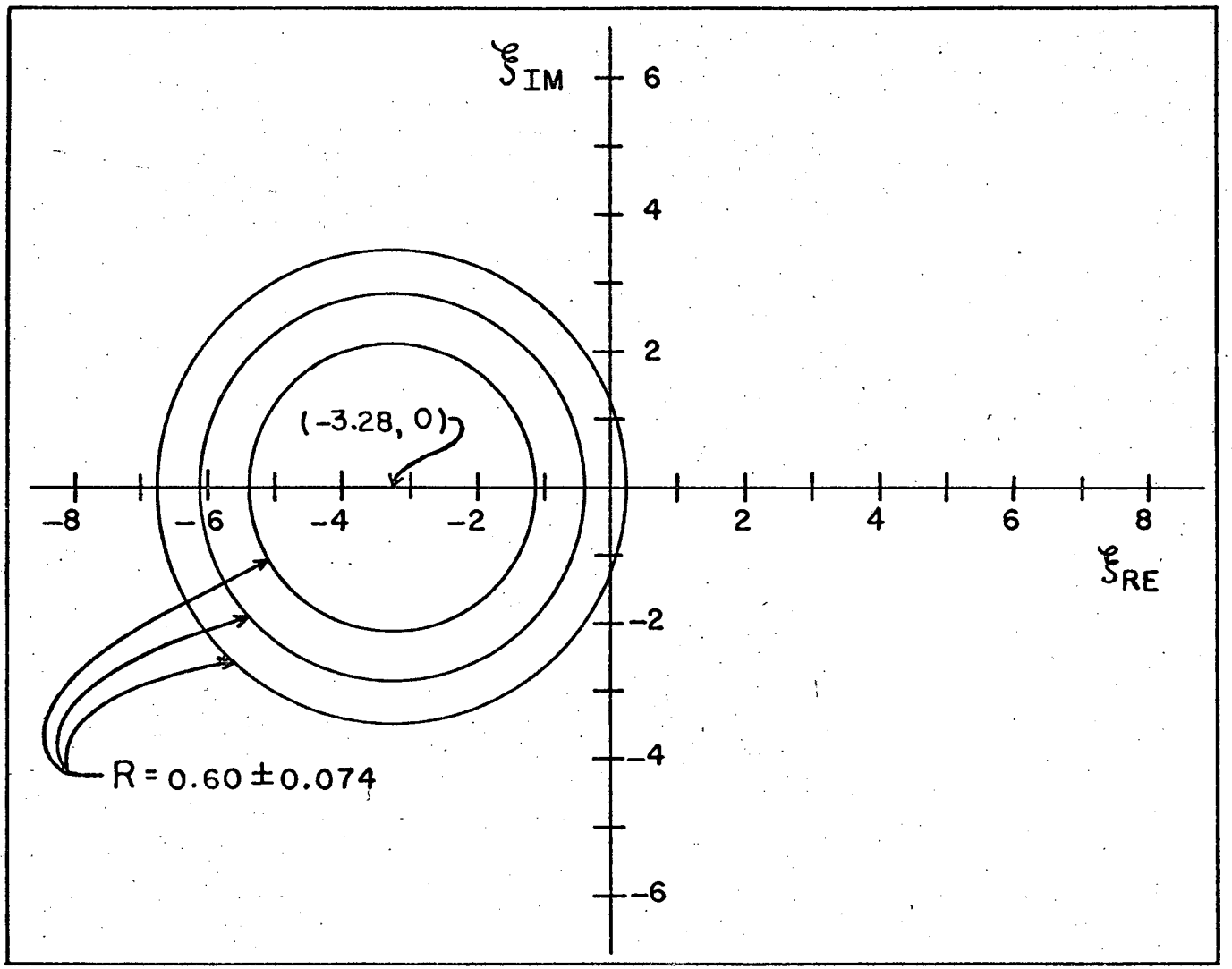

Fig. 19. A plot showing the relationship between ξ_{RE} and ξ_{IM} as a function of the experimentally determined ratio $R = BR_{K_{\mu 3}}/BR_{K_{e3}}$.

This report was prepared as an account of Government sponsored work. Neither the United States, nor the Commission, nor any person acting on behalf of the Commission:

A. Makes any warranty or representation, expressed or implied, with respect to the accuracy, completeness, or usefulness of the information contained in this report, or that the use of any information, apparatus, method, or process disclosed in this report may not infringe privately owned rights; or

B. Assumes any liabilities with respect to the use of, or for damages resulting from the use of any information, apparatus, method, or process disclosed in this report.

As used in the above, "person acting on behalf of the Commission" includes any employee or contractor of the Commission, or employee of such contractor, to the extent that such employee or contractor of the Commission, or employee of such contractor prepares, disseminates, or provides access to, any information pursuant to his employment or contract with the Commission, or his employment with such contractor.